July 15, 2025
Volume 59
Number 27
pubs.acs.org/est

Environmental Science & Technology

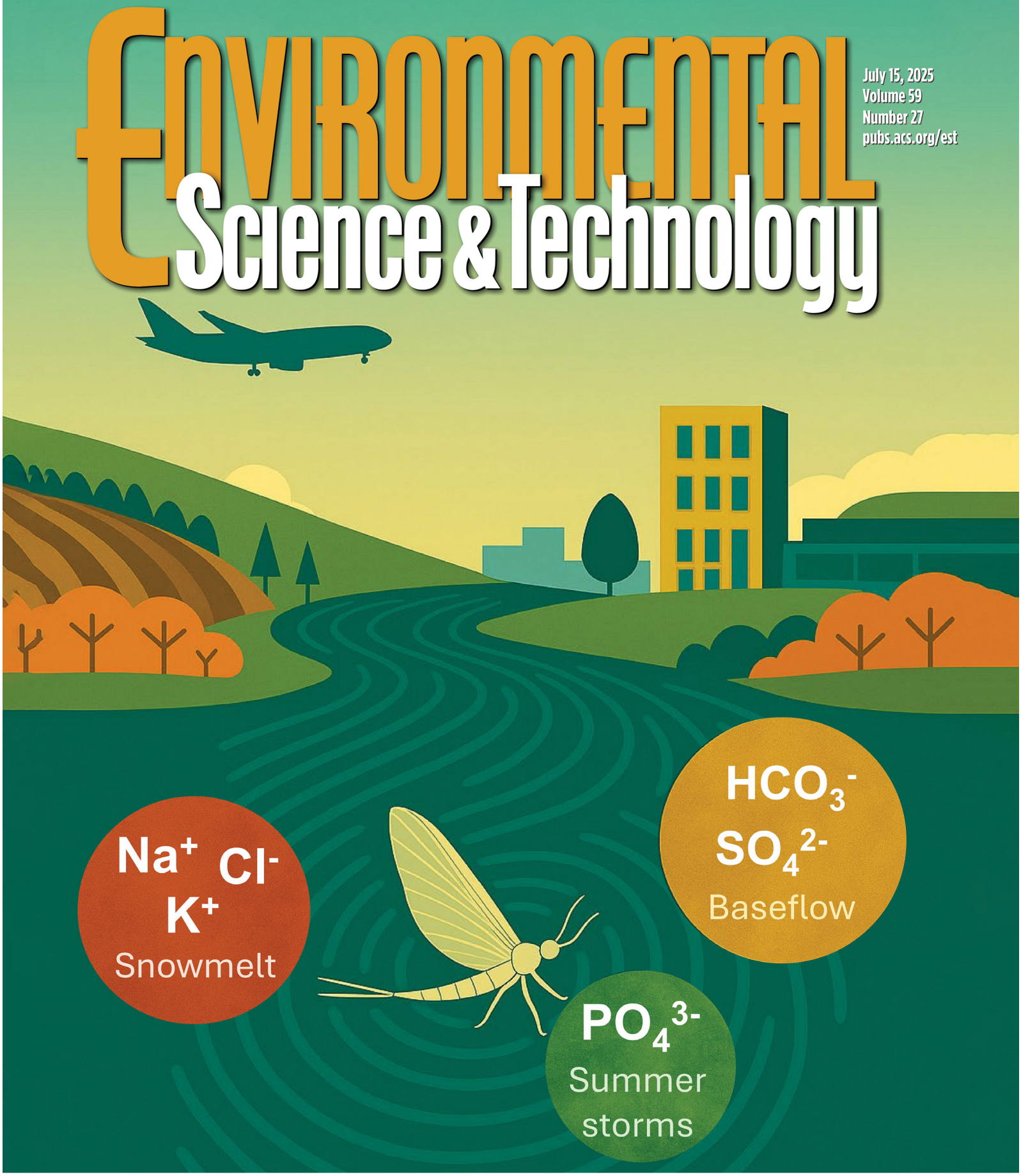

ACS Publications
Most Trusted. Most Cited. Most Read.

www.acs.org

Environmental Science & Technology

pubs.acs.org/est

Article

Ion Clusters Reveal the Sources, Impacts, and Drivers of Freshwater Salinization

Diver E. Marin, Stanley B. Grant,* Shantanu V. Bhide, Megan A. Rippy, Jesus D. Gomez-Velez, Robert N. Brent, Sujay S. Kaushal, Harold Post, Sydney Shelton, Shalini Misra, Erin R. Hotchkiss, Ahmed Monofy, Dongmei Alvi, Bradley Schmitz, Shannon Curtis, Christina C. Davis, Peter Vikesland, and Admin Husic

Cite This: *Environ. Sci. Technol.* 2025, 59, 14053−14062

Read Online

ACCESS | Metrics & More | Article Recommendations | Supporting Information

ABSTRACT: Population growth, land use change, climate change, and natural resource extraction are driving the salinization of freshwater resources worldwide. Reversing these trends will require data-centric approaches that identify salt sources, environmental drivers, and ecosystem responses. In this study, we applied principal component analysis and hierarchical clustering to identify ion covariance patterns, or "ion clusters," in Broad Run, an urban stream in the Mid-Atlantic United States. These clusters correspond to distinct hydrologic regimes and reveal specific salinization risks: (1) phosphorus pollution mobilized during summer storms (Cluster 1); (2) elevated concentrations of sulfate and bicarbonate during baseflow (Cluster 2), likely reflecting groundwater discharge; and (3) elevated specific conductance and sodium, chloride, and potassium ion concentrations during snowmelt and rain-on-snow events (Cluster 3), driven by deicer and anti-icer wash-off. These ion fingerprints offer a transferable framework for diagnosing salt sources, assessing ecological risk, and identifying management targets. Our findings underscore the need for next-generation stormwater infrastructure and smart growth policies to protect aquatic life in rapidly urbanizing watersheds.

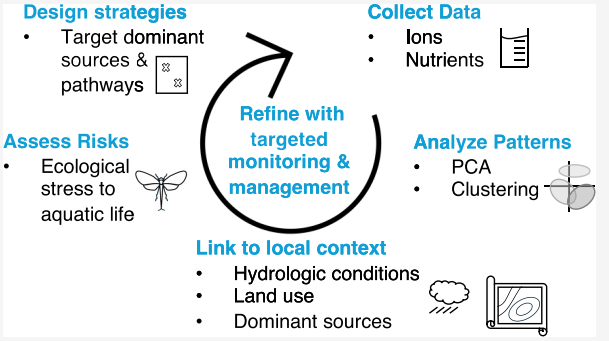

KEYWORDS: *salinization, streams, urbanization, stormwater, ecology, groundwater, deicers*

INTRODUCTION

Dissolved ions occur naturally in freshwater systems due to atmospheric deposition[1] and the weathering of soils and bedrock.[2] Yet across the globe, salinity levels in rivers, streams, lakes, and groundwater are rising due to human activities.[3] In temperate urban and suburban areas, these changes are driven by overlapping inputs from road deicers, construction materials, fertilizers, storm runoff, and treated wastewater.[3−8] As a result, ion concentrations are increasing even in regions without historic salinization issues,[9] prompting concern about ecological degradation and long-term sustainability.[10]

Salinization can reduce freshwater biodiversity and ecosystem function[11−13] with impacts ranging from osmotic stress for sensitive species to the mobilization of legacy pollutants.[14−17] While regulatory efforts have historically focused on single-ion thresholds (e.g., chloride[18]) or aggregate metrics (e.g., specific conductance[19]), emerging research highlights the importance of ion mixtures and their interactions.[20,21] These mixtures can differ substantially across space and time depending on the source, transport pathway, and hydrologic context.[22]

In this study, we investigate patterns of stream salinization in Broad Run, a rapidly urbanized watershed in Northern Virginia. Using 3 years of stream monitoring data, we apply principal component analysis (PCA) and hierarchical clustering to identify groups of samples with similar ion covariance patterns, which we refer to as *ion clusters*. We interpret these clusters with respect to seasonal hydrologic conditions and use them to evaluate potential sources, ecological risks, and management strategies.

This study is novel in its use of ion clustering as an organizing framework for diagnosing salinity drivers and their impacts on stream ecosystems. We hypothesize that distinct ion mixtures reflect not only salt source types but also transport mechanisms and retention times, which vary seasonally and across flow regimes. Specifically, we ask: (1) What are the statistically distinct ion mixtures in this urban stream, and how do they relate to hydrologic conditions? (2)

Received: April 4, 2025
Revised: June 4, 2025
Accepted: June 5, 2025
Published: June 16, 2025

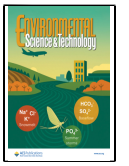

What do these mixtures reveal about the likely sources and pathways of salinity inputs? (3) How do ion mixtures relate to aquatic life stress, as inferred from regional bioassessment thresholds? By addressing these questions, we demonstrate how statistical pattern recognition tools can reveal actionable insights for managing freshwater salinization in urbanizing watersheds.

MATERIALS AND METHODS

Site Description. Our monitoring station (BL30; 39.024°N, 77.439°W) is located on a fourth-order reach of Broad Run in the Potomac-Shenandoah River Basin (Figure S1 and Note S1). This portion of Broad Run drains a rapidly urbanizing 152 km^2 catchment in Loudoun County, Virginia, USA. Impervious cover in this subwatershed increased from approximately 19% in 2001 to approximately 32% in 2019.[23] The drainage lies within the Mesozoic Lowlands hydrogeomorphic region, underlain by siltstone, shale, sandstone, diabase, and basaltic rock types[24,25] (Figures S2 and S3). There are no wastewater treatment plant discharges upstream of BL30.

Sample Collection and Field Measurements. Baseflow and storm samples were collected at BL30 over a three-year period (2020-04-13 to 2023-05-03). Biweekly grab samples were collected to represent the relatively stable conditions of baseflow, whereas flow-weighted composite samples were used to capture representative pollutant concentrations during storm events, when concentrations can vary considerably over the storm hydrograph.[26] All water samples were transported on ice to the Occoquan Watershed Monitoring Laboratory either immediately (baseflow) or within 24 h (storm samples) of collection. Field measurements of streamwater temperature, pH, specific conductance (SC), and total alkalinity were conducted during baseflow sampling. For safety reasons, no field measurements were conducted during storm events (Note S2).

Laboratory Analysis. *Dissolved Ions.* Filtered baseflow and storm samples were analyzed within 1 day of arrival at the laboratory for major dissolved ions (K^+, Na^+, Cl^-, SO_4^{2-}, Ca^{2+}, Mg^{2+}) using ion chromatography (Dionex ICS-5000) following ASTM D6919-09 and SM 4110 B-2011. In baseflow samples, bicarbonate concentrations were calculated from field-measured alkalinity (Notes S3 and S4).

Nutrients. Unfiltered samples were analyzed for total nitrogen (TN) and total phosphorus (TP) following persulfate digestion. Filtered subsamples were analyzed for dissolved nitrate + nitrite (NO_3^-/NO_2^-) and orthophosphate (PO_4^{3-}) using Astoria Pacific autoanalyzers and Standard Methods 4500-P J-2011, 4500-NO_3^- F-2011, and 4500-P F-2011. Additional details, including sample preservation, instrumentation, and detection limits, are provided in Note S3 and Table S3.

Total Suspended Solids. Total suspended solids (TSS) were measured gravimetrically, following Standard Method 2540 D-2011.

Left-Censored Values and Charge Balance Error (CBE). All left-censored values (i.e., values below the limit of detection (LOD), Table S3) were set equal to one-half the LOD. Charge balance error (CBE) was calculated for each sample based on the normality of all measured or imputed cations (K^+, Na^+, Ca^{2+}, Mg^{2+}, NH_4^+, H^+) and anions (HCO_3^-, Cl^-, SO_4^{2-}, NO_3^-/NO_2^-, PO_4^{3-}) as described in Note S5.

Imputation of Missing Data. Missing values were imputed using regularized iterative Principal Component Analysis (PCA) via the `estim_ncp` and `imputePCA` functions in the MissMDA package (R, version 4.4.1). The `estim_ncp` function estimates the optimal number of principal components which are then used by `imputePCA` to perform the imputation.[27] Imputed bicarbonate concentrations in storm samples were validated using two approaches: (1) comparison to bicarbonate concentrations estimated via a geochemical charge-balance method, in which all unbalanced anionic charge is attributed to bicarbonate (Note S4); and (2) evaluation of CBE calculated from the measured and imputed ion concentrations for each storm sample (Note S5).

Environmental Variables. *Stream Discharge.* Stream discharge was estimated from hourly stage measurements collected with a pressure transducer (Pressure Systems, Inc., 10 PSI Transducers) fixed to a wooden monument near the stream bank, just upstream of a stable cross-section provided by a sewer line crossing. Stage measurements were converted to discharge, stored in a data logger (Sutron 8210), and retrieved during baseflow sample collection. Hourly stream discharge measurements were averaged to daily discharge for further analysis (Note S6). The stage-discharge relationship was updated every 3 to 6 months (and after large storms) following USGS Method 3-A8.[28]

Baseflow Index (BFI). Daily estimates of baseflow, Q_{BF}, were computed by applying a Recursive Digital Filter to the measured discharge data, Q (grwat package in R Software, version 4.4.1, R Core Team 2024)[29,30] (Note S7). The baseflow index was calculated as BFI = Q_{BF}/Q.

Precipitation, Air Temperature, and Snow Melt. Hourly precipitation and air temperature data were collected from the weather station at Dulles International Airport (located within the drainage area, 10 km to the south of BL30) (Note S6). Snowmelt was estimated using the Hydrologiska Byråns Vattenbalansavdelning (HBV) model[31,32] (Note S8).

Local Groundwater Data. Groundwater data were obtained from the U.S. Geological Survey's National Water-Quality Assessment (NAWQA) program.[33] Specifically, we accessed records from USGS well no. 385930077215901, located approximately 7 km southeast of BL30 (Figure S2). Between 2003 and 2015, the USGS collected eight samples from this well (at depths of 20−90 feet below ground surface) and analyzed them for the same suite of inorganic ions and nutrients described above for Broad Run.

Principal Component Analysis (PCA) and Hierarchical Clustering. Prior to PCA, ion and nutrient concentrations were log-transformed to reduce skewness and standardized (Z-scored). The number of significant principal components (PCs) was determined using a resampling-based stopping rule, which identifies components that explain more variance than expected by chance ($p < 0.05$)[34,35] (Figure S8 and Note S9).

Hierarchical clustering was then applied in principal component space using Euclidean distance and the Ward criterion, as implemented in the `HCPC` function from the FactoMineR package (R version 4.4.1).[36] The optimal number of clusters was identified based on the relative loss of inertia (i.e., within-cluster variance), with the selected partition corresponding to the point at which additional clusters result in a substantially smaller gain in explanatory power. Permutational multivariate analysis of variance (perMANOVA) with Euclidean distance was used to test for statistically significant differences among the identified clusters.[37] As a visual guide,

https://doi.org/10.1021/acs.est.5c04512
Environ. Sci. Technol. 2025, 59, 14053−14062

ellipses were drawn to represent the approximate region of principal component space occupied by each cluster; specifically, each ellipse represents the region of principal component space that would be expected to include 90% of samples associated with a particular cluster, assuming a multivariate normal distribution of the samples within each cluster.

Median Comparison Tests. Nonparametric bootstrapping was used to test for significant differences in group medians (using the `boot` package in R version 4.4.1).[38] Significance was assessed at the $p < 0.05$ level using bias-corrected and accelerated confidence intervals, with adjustments for multiple comparisons made using the Bonferroni correction.[39]

Benthic Macroinvertebrate Responses. Since 2001, the Virginia Department of Environmental Quality (VDEQ) has collected stream ion concentrations and biological integrity metrics—including the Virginia Stream Condition Index[40]—at 473 randomly selected monitoring stations across the state as part of its probability-based monitoring program.[41] To contextualize the measurements at BL30, we compared them to (1) concentrations measured at the VDEQ probability-based monitoring sites within the Northern Piedmont Ecoregion (for ecoregion-specific percentiles) and (2) statewide aquatic life stress thresholds established by the VDEQ, which are currently not available at a finer ecoregional resolution (see Note S10 for details).

First, for each ion and nutrient measurement at BL30, we calculated its percentile ranking relative to concentrations measured at VDEQ monitoring sites within the Northern Piedmont Ecoregion, where BL30 is located, on the premise that stream stations within the same ecoregion will support similar macroinvertebrate assemblages and exhibit responses similar to those of environmental stressors.

Second, we compared the ion and nutrient concentrations at BL30 to statewide benthic community response thresholds developed by VDEQ.[41] These thresholds, derived from the agency's probabilistic monitoring data set using quantile regression and conditional probability analyses,[42] define concentration ranges associated with increasing probability of stress to aquatic life across all Virginia ecoregions: "No Probable Stress" (background conditions), "Low Probability of Stress" (minor biological response), "Medium Probability of Stress" (substantial biological response), and "High Probability of Stress" (significant degradation of the benthic community).

RESULTS

Stream Flow. Stream discharge at BL30 ranged from 0.113 to 4.94 mm/day during baseflow sampling (median = 0.310 mm/day) and from 1.59 to 22.0 mm/day during storm sampling (median= 5.48 mm/day).

Water Quality Data Set. A balanced number of baseflow ($N = 79$) and storm ($N = 74$) samples were collected at BL30 over the three-year study period. After the imputation of missing values, four samples (two baseflow and two storm) had an absolute charge balance error (CBE) >10% and were excluded from further analysis (Note S5). The remaining samples ($N = 149$) had CBEs ranging from −4.37% to +6.23% (baseflow samples, $N = 77$) and from −4.2% to +7.01% (storm samples, $N = 72$).

Ion concentrations were generally above their lower limits of detection (LODs). The exceptions were NH_4^+ and PO_4^{3-}, which were below their respective LODs in 2 and 27 samples, respectively.

The final data set included 2,086 measured and 179 imputed values for specific conductance (SC), total phosphorus (TP), total nitrogen (TN), total suspended solids (TSS), and dissolved inorganic cations (Ca^{2+}, Mg^{2+}, NH_4^+, K^+, Na^+, H^+) and anions (Cl^-, SO_4^{2-}, NO_3^-/NO_2^-, PO_4^{3-}, HCO_3^-).

Principal Component Analysis (PCA). PCA was performed on measured or imputed concentrations of cations (Ca^{2+}, Mg^{2+}, K^+, Na^+, NH_4^+, H^+) and anions (Cl^-, SO_4^{2-}, NO_3^-/NO_2^-, HCO_3^-); because a relatively large number of PO_4^{3-} measurements were left censored (see last section), this ion was not included in the PCA. The goal of the PCA was to identify statistically distinct ion covariance patterns, and therefore bulk nutrients (TP and TN) and TSS measurements were also not included in the analysis.

Two significant principal components explained 73% of the total variance in ion measurements (Figure 1). The first

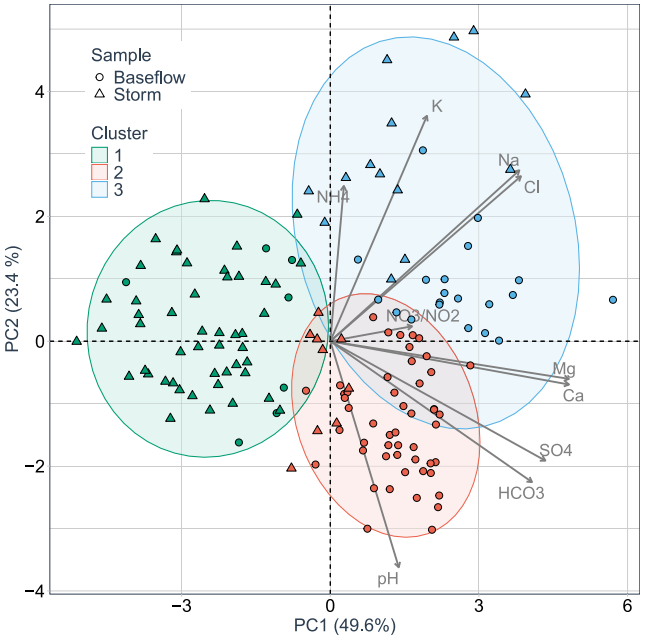

Figure 1. 73% of the variance in ion concentrations measured at Broad Run is captured by the two principal components PC1 (49.6%) and PC2 (23.4%). The position in biplot space of all $N = 77$ baseflow samples (circles) and $N = 72$ storm samples (triangles) are shown, along with loadings for the ions included in the PCA (Ca^{2+}, Mg^{2+}, NH_4^+, K^+, Na^+, pH, Cl^-, SO_4^{2-}, NO_3^-/NO_2^-, HCO_3^-). The colored ellipses are included here only as a visual aid; the actual boundary between clusters is not elliptical. Importantly, despite some overlap between ellipses, the hierarchical clustering method assigned each baseflow and storm sample to one of three clusters (Cluster 1, 2, or 3). Results from the perMANOVA test indicate that the three clusters are significantly different ($p < 0.05$).

principal component (PC1) reflects overall ion concentration, with samples scoring positively along PC1 characterized by elevated ion levels (gray arrows in the figure). The second principal component (PC2) differentiates between samples enriched in monovalent ions (positive PC2) and samples enriched in divalent ions and carbonate system constituents (negative PC2).

Hierarchical Cluster Analysis. Hierarchical clustering in principal component space identified three statistically distinct ion covariance patterns, or ion clusters, associated with the samples collected at BL30 (Figure 1). As documented below,

https://doi.org/10.1021/acs.est.5c04512
Environ. Sci. Technol. 2025, 59, 14053−14062

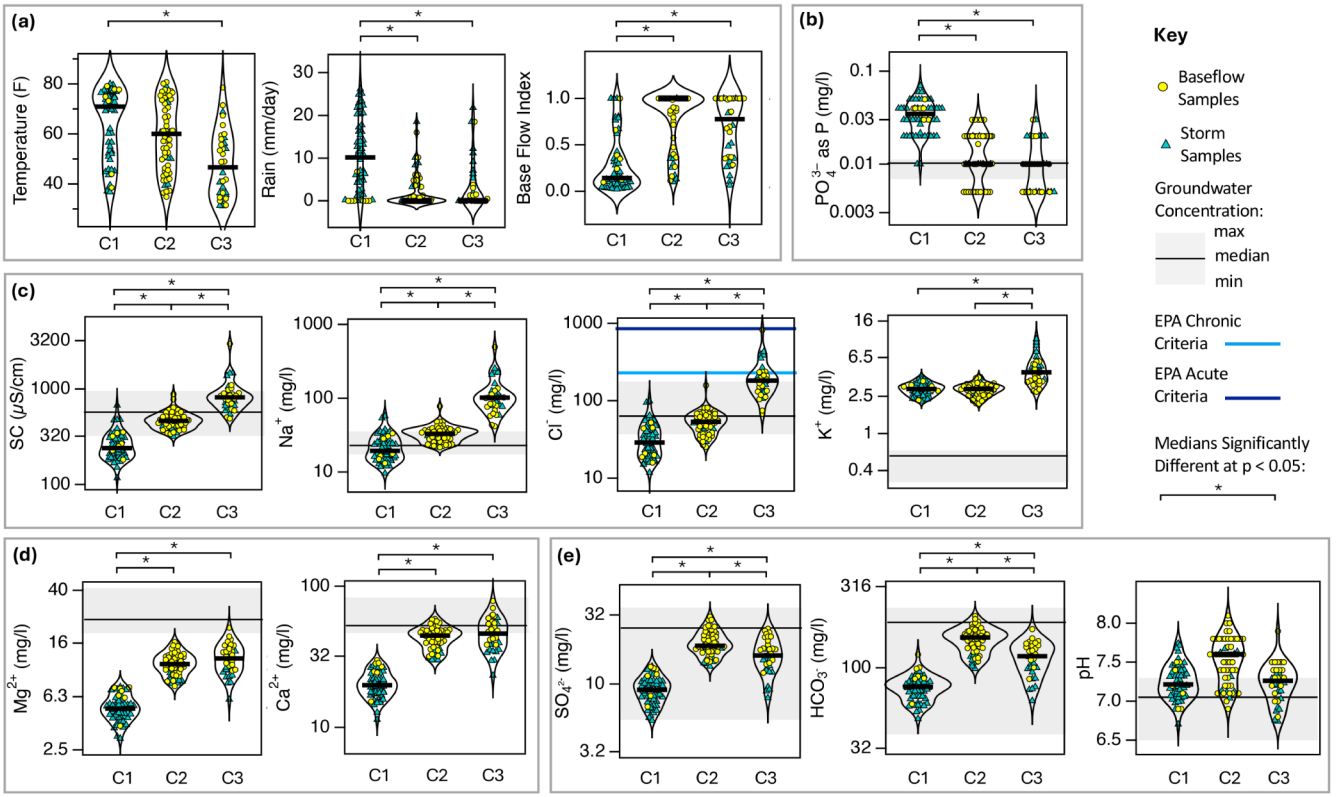

Figure 2. Violin plots of the (a) environmental drivers and (b)−(e) ion concentrations associated with each of the three clusters (C1 = Cluster 1 (summer storms), C2 = Cluster 2 (baseflow), and C3 = Cluster 3 (snowmelt and rain-on-snow events)). Ion concentrations are divided into those for which the median concentrations are highest in (b) C1, (c) C3, (d) C2 and C3, or (e) C2. The median concentrations for each ion are indicated by a thick black horizontal line. Baseflow and storm samples are indicated by yellow circles and teal triangles, respectively. Any pair of median values are significantly different (at $p < 0.05$) when connected by starred brackets. Thin black horizontal line and gray region denotes the median and range of ion concentrations measured in a nearby groundwater well. Orthophosphate concentrations below the limit of detection (LOD) of 0.01 mg/L were set to one-half the LOD. Values of pH, SC, and HCO_3^- in storm samples were imputed.

these three ion clusters correspond to (1) summer storm events (Cluster 1), (2) summer and winter baseflow conditions (Cluster 2), and (3) winter snowmelt and rain-on-snow events (Cluster 3).

Environmental Drivers. Cluster 1 is primarily composed of samples collected during summer storm events, as indicated by the high proportion of storm samples, elevated median air temperature and rainfall, and a baseflow index (BFI) near zero (Figure 2a).

Cluster 2 is primarily composed of summer and winter baseflow samples, characterized by a median BFI near unity, low median rainfall, and a wide range of air temperatures (Figure 2a).

Cluster 3 is primarily composed of samples collected during winter snowmelt or rain-on-snow events—a common condition in this region. These samples are marked by low median air temperatures, low median rainfall, intermediate median BFI, and timing consistent with snowmelt predictions from the HBV model (10 of 31 Cluster 3 samples occurred during modeled snowmelt periods; data not shown) (Figure 2a).

Geochemical Signatures. Samples in Cluster 1 are characterized by relatively low median concentrations of most ions, consistent with the dilution by urban runoff during summer storm events (Figure 2c−e). Two exceptions are orthophosphate (PO_4^{3-}) and potassium (K^+) ion concentrations (Figure 2b,c). Potassium ion concentrations are particularly elevated during winter deicing events (Cluster 3) but remain high (relative to groundwater) during both baseflow conditions and summer storms (Clusters 2 and 1). Orthophosphate exhibits substantially higher concentrations in Cluster 1 than in either groundwater or the other two clusters (Figure 2b). PO_4^{3-} is also weakly correlated with TSS in Cluster 1 samples (Pearson's $R = 0.34$, $p < 0.05$, data not shown).

Samples in Cluster 3 exhibit elevated specific conductance (SC) and markedly higher median concentrations of sodium and chloride compared to the other clusters (Figure 2c), consistent with the wash-off of NaCl-based road deicers and anti-icers during snowmelt or rain-on-snow events.

DISCUSSION

The three ion clusters identified above reflect distinct hydrologic regimes and geochemical signatures. In this section, we explore their implications for: (1) identifying potential salt sources; (2) assessing risks to aquatic life in Broad Run; and (3) management actions and monitoring strategies.

Diagnosing Watershed Salinity Sources. The hydrologic and geochemical characteristics associated with each ion cluster provide useful information for diagnosing salt sources and biogeochemical processes in urban watersheds. In this section, we focus on how relationships among ion concentrations, including how the molar concentration of one ion changes relative to another within a cluster, can offer insights into the drivers of freshwater salinization. We use this approach to evaluate four potential sources of salinity at BL30: (1)

https://doi.org/10.1021/acs.est.5c04512
Environ. Sci. Technol. 2025, 59, 14053−14062

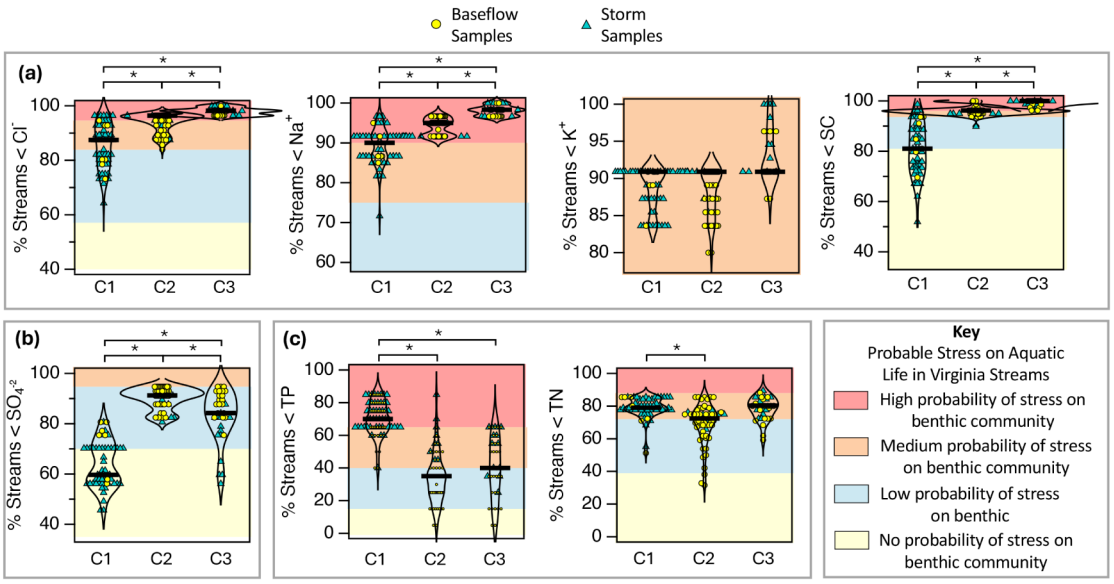

Figure 3. Contextualizing water quality in Broad Run and inferred probability of stress to aquatic life by cluster (C1 = Cluster 1 (summer storms), C2 = Cluster 2 (baseflow), and C3 = Cluster 3 (snowmelt and rain-on-snow events)). (a) Percentile ranking of chloride, sodium, potassium, and SC levels measured in samples collected from Broad Run (yellow circles or green triangles) relative to corresponding chloride, sodium, potassium, and SC levels measured by VDEQ in Northern Piedmont Ecoregion streams (vertical axis). Color in each plot indicates the inferred probability of stress to aquatic life (see the color key and text). The percentile rankings and inferred probabilities for aquatic life stress are highest for Broad Run samples collected during snowmelt or rain-on-snow events (Cluster 3). (b) Percentiles and inferred probability of stress on aquatic life for sulfate measurements on Broad Run. (c) Percentiles and inferred probability of stress on aquatic life for nutrients TP and TN.

sodium- and chloride-based road deicers, (2) potassium-based airport deicers, (3) calcium- and magnesium-based deicers, and (4) natural mineral sources associated with the local Triassic basin geology.

Sodium- and Chloride-Based Road Deicers. The strong molar relationship between Na and Cl across all clusters (Pearson's Correlation R = 0.99, 0.98, and 0.99 for Clusters 1, 2, and 3, respectively) points to NaCl-based deicers as a plausible salt source at BL30 (Figure S9a). Cross-plotting measured sodium and chloride concentrations, we find that the resulting slopes (i.e., $\Delta Na^+/\Delta Cl^-$, where the symbol Δ denotes change) approach the 1:1 molar ratio expected for rock salt in the following order: Cluster 2 (0.68 ± 0.04), Cluster 1 (0.83 ± 0.02), and Cluster 3 (0.92 ± 0.03) (see Note S11). The lowest slope occurs under summer baseflow conditions (Cluster 2), when deicers are not being applied and transit times through the watershed are relatively long.[43] The highest slope occurs during winter (Cluster 3), when deicer use is more likely. These patterns are consistent with NaCl inputs along with cation exchange processes that preferentially retard sodium transport (relative to chloride), leading to observed slopes <1 across all flow and seasonal conditions.[2−45]

While elevated concentrations of sodium and chloride during baseflow (Cluster 2) may reflect a combination of natural sources (such as mineral weathering from Triassic basin sediments,[46] see below) and legacy impacts from past deicer applications that have infiltrated to groundwater,[47] the extremely high concentrations observed during snowmelt and rain-on-snow events (Cluster 3) are more clearly attributable to recent applications of road salt and anti-icing agents.

Potassium-Based Airport Deicers. A likely source of potassium in Broad Run is potassium-based deicers used at Washington Dulles International Airport, a major regional facility serving over 24 million travelers annually.[48] Because chloride salts are corrosive to aircraft, the U.S. Federal Aviation Administration permits alternatives such as potassium acetate and potassium formate, which are widely used in the aviation industry.[49]

Unlike NaCl, these potassium-based deicers lack inorganic counterions, making ion slope analysis infeasible given the set of ions measured here. However, useful information can still be gleaned from the clusters. For example, a possible alternative (nondeicer) source of potassium is the widely used fertilizer, KCl. However, the highest potassium concentrations at BL30 are associated with snowmelt and rain-on-snow events (Cluster 3, Figure 2c) when fertilizer use would be extremely unlikely. As noted earlier, potassium does not exhibit the dilution response seen for most other ions. While median K^+ concentrations are highest in Cluster 3, they remain elevated (relative to groundwater) in both Clusters 1 and 2 (Figure 2c).

Two of the airport's four runways drain into Broad Run, both directly through a stormwater conveyance system and indirectly via a detention pond (Figure S1). The elevated potassium concentrations observed in Cluster 3 would be consistent with inputs from the first flow path during snowmelt or rain-on-snow events. In contrast, the persistently high values in Clusters 1 and 2 are more consistent with the gradual release of potassium from the airport detention pond.

Calcium- and Magnesium-Based Deicers. Calcium and magnesium are active ingredients in several anti-icing products, including calcium chloride, magnesium chloride, and calcium magnesium acetate (CMA).[21,50] Calcium and magnesium from the first two deicers would be expected to covary with chloride in a 1:2 molar ratio. However, Pearson correlation coefficients between Ca^{2+} and Cl^- and between Mg^{2+} and Cl^- are low (R < 0.52) across all clusters, and the corresponding slopes are not significantly different from zero (Figures S9b,c).

CMA ($Mg_2Ca(OAc)_6$) would be expected to yield a 2:1 molar increase in magnesium relative to calcium.[51] However,

https://doi.org/10.1021/acs.est.5c04512
Environ. Sci. Technol. 2025, 59, 14053−14062

while Mg^{2+} and Ca^{2+} are strongly correlated at BL30 ($R \geq 0.96$), the observed Mg:Ca slope is approximately 0.4 (1:2.5), inconsistent with the molecular formula of CMA (Figure S9d). These patterns suggest that calcium and magnesium are not primarily derived from deicers, pointing instead to geogenic sources consistent with the local Triassic basin geology discussed next.

Triassic Basin Sediments. Across all clusters, calcium and magnesium are strongly correlated with sulfate ($R > 0.85$) and bicarbonate ($R > 0.77$) (Figure S10a–d). The inferred slopes ($\Delta Ca^{2+}/\Delta SO_4^{2-}$ = 3.74 to 5.73, $\Delta Ca^{2+}/\Delta HCO_3^-$ = 0.40 to 0.55, $\Delta Mg^{2+}/\Delta SO_4^{2-}$ = 1.9 to 2.5, and $\Delta Mg^{2+}/\Delta HCO_3^-$ = 0.17 to 0.25) are similar to the corresponding median (4.9, 0.42, 3.7, 0.32, respectively) and average (5.4, 0.50, 4.1, 0.38, respectively) ratios of ion concentrations measured in the local groundwater. Further, across all three clusters, the magnesium-to-calcium ratio measured in groundwater (both median and average equal to 0.76) is close to the 1:2.5 ratio inferred for the stream ($\Delta Mg^{2+}/\Delta Ca^{2+}$ = 0.43 to 0.45) (Figure S9d). These results are also consistent with USGS groundwater data from nearby Fairfax County,[46,52,53] which indicate that groundwater in the underlying Triassic basin sediments is predominantly calcium–magnesium type, with elevated sulfate concentrations likely derived from gypsum in the rock matrix.[54]

Diagnosing Potential Salinity Stressors to Aquatic Life in Streams. The three ion clusters can also be linked to statewide thresholds for aquatic life stress, providing a framework for identifying likely targets for management action.[15,55,56]

The probability that chloride, sodium, and specific conductance (SC) measurements at BL30 pose stress to aquatic life ranges from low to high in Cluster 1, medium to high in Cluster 2, and consistently high in Cluster 3 (Figure 3a). Across all clusters, potassium concentrations correspond to a medium probability of stress.

Sulfate, despite being elevated during baseflow (Cluster 2), is associated with mostly low or no probability of aquatic life stress (Figure 3b). TP, in contrast, poses a high probability of stress during summer storm events (Cluster 1; Figure 3c). Because TP is highly correlated with both TSS (Pearson's R = 0.86, $p < 0.05$) and flow (R = 0.62, $p < 0.05$), the ultimate cause of risk to benthic invertebrate assemblages is likely habitat disruption and sediment erosion associated with high-flow events.[57] TN concentrations fall mostly in the low to medium risk range across all clusters (Figure 3c).

Together, these results point to three primary risk scenarios for salt-sensitive macroinvertebrates such as mayflies, stoneflies, and caddisflies, particularly during vulnerable life stages:[14,15,58,59] (1) high phosphorus concentrations and associated sediment mobilization and benthic habitat disturbance during summer storms (Cluster 1); (2) somewhat elevated chloride, sodium, and SC under baseflow conditions (Cluster 2), perhaps associated with legacy deicer use; and (3) very high levels of chloride, sodium, potassium, and SC during snowmelt and rain-on-snow events associated with active deicer use (Cluster 3). These findings are consistent with low biotic and Stream Condition Index (SCI) scores in urban streams in the region,[15,60] including Accotink Creek in neighboring Fairfax County, for which chlorides from deicers have been identified as a primary stressor.[61]

Low SCI scores in Broad Run have resulted in its recent listing as impaired for aquatic life uses by VDEQ.[62,63] Upon completion of the required stressor identification study, salinity is likely to again be identified as a primary aquatic life stressor in this urbanized watershed, for which management actions will be required. By directly relating our ion measurements to VDEQ's aquatic life stress thresholds, the results presented here should help local jurisdictions, state agencies, and natural resource managers prioritize monitoring efforts, particularly under resource constraints, and focus on the ion mixtures and hydrologic regimes most likely to affect the biological integrity of Broad Run.[64]

Watershed-Based Integrated Management. The statistical pattern recognition tools employed here offer a new "tool-in-the-toolbox" for designing targeted streamwater quality management actions. Further, these tools provide a statistically grounded alternative to subjective sample classification based on presumed hydrologic regimes (e.g., see Figure S12) and may be particularly useful in settings where discharge data are unavailable or uncertain. Our findings suggest at least three key opportunities for improved streamwater quality management at BL30.

Targeting Seasonal Flow Regimes for Monitoring and Nutrient Reduction. Clusters defined by patterns in stream ion chemistry reveal when and how risks to aquatic life and downstream uses arise. For example, phosphorus concentrations pose risks to aquatic life during summer storms (Cluster 1), suggesting that storm-driven erosion and sediment transport are key phosphorus sources.[65] Riparian buffers, street sweeping, and stormwater controls such as bioretention or filtration basins could be deployed to reduce particulate and particle-bound phosphorus loads.[65]

Confirming Source Hypotheses with Targeted Monitoring. The elevated potassium concentrations observed in Cluster 3 (snowmelt events) and persistent potassium signals in Clusters 1 and 2 suggest both event-driven and delayed contributions from airport deicers. To confirm this source attribution, follow-up grab sampling immediately downstream of the airport, timed with winter deicing events and summer pond drawdowns, could help trace potassium acetate/formate usage. Similarly, a focused winter sampling campaign at road-adjacent outfalls could help verify whether NaCl-based deicers explain the elevated chloride and specific conductance values in Cluster 3.

Supporting Smart Growth and Best Management Practices. By resolving overlapping sources through ion ratios and covariance patterns, our results can also inform efforts to reduce salt inputs to streams via smart growth strategies and best management practices (BMPs).

Riparian and conservation zones are a smart growth strategy that mitigate salt pollution,[22,66] attenuating ions through plant uptake, ion exchange, and biogeochemical cycling. Their effectiveness depends on factors such as buffer width, vegetation type, and site-specific conditions.[67] Our ion clusters reveal that ion and nutrient concentrations and their implied risks to aquatic life vary seasonally. For instance, phosphorus concentrations are highest during summer storms (Cluster 1), whereas ions linked to deicers and anti-icers peak during winter snowmelt and rain-on-snow events (Cluster 3). These patterns can inform hypotheses about dominant nutrient and salt attenuation mechanisms in riparian and conservation zones—for example, plant uptake of phosphorus during the growing season and soil-mediated ion exchange during winter months—for future evaluation.

While traditional BMPs were designed primarily to reduce peak flows,[68] modern green infrastructure—including green

https://doi.org/10.1021/acs.est.5c04512
Environ. Sci. Technol. 2025, 59, 14053–14062

roofs, permeable pavements, bioswales, and bioinfiltration systems—can also reduce sediment, phosphorus, and bacterial loading during storms.[69,70]

The next generation of these systems could also target dissolved salts, for example, by incorporating ion-exchange media or real-time monitoring and control systems to capture salt in runoff from roads and parking lots during deicer washoff events (Cluster 3).[71−73] For example, Long et al.[74] recently reported that cattails in a standard-sized highway detention basin (2000−3000 m^2) could remove up to 200 kg of deicer-associated Cl^- per year. Alternatively, high-frequency specific conductance sensors could trigger retention of salt-rich runoff when conductivity spikes,[75−77] followed by longer-term treatment (e.g., phytoremediation[74]) or controlled disposal (e.g., pump-and-haul). Retained runoff could also be gradually released during subsequent deicer-free storms, effectively diluting the water of Cluster 3 with the water of Cluster 1.

Information gleaned from the ion clusters could also help local jurisdictions select locally tailored deicing formulas likely to have the least impact on aquatic life, for example, by mimicking ion mixtures already contributed to streams by the local geology. However, for these bespoke deicers to be effective, the applied concentrations of individual ions would still need to be high enough to achieve a desired eutectic temperature.[78]

While further research is needed to evaluate the feasibility, scalability, costs, and potential unintended consequences of these strategies,[5,70,74,79] the ion covariance patterns identified through ordination and clustering offer a powerful starting point for generating hypotheses and guiding the design of next-generation solutions to reverse freshwater salinization.

■ ASSOCIATED CONTENT

Supporting Information

The Supporting Information is available free of charge at https://pubs.acs.org/doi/10.1021/acs.est.5c04512.

Notes S1−S13, including figures and tables, provide additional details on watershed characteristics, water quality analyses, statistical methods, hydrologic and ecological data, and concentration-discharge relationships (PDF)

■ AUTHOR INFORMATION

Corresponding Author

Stanley B. Grant − *Occoquan Watershed Monitoring Laboratory, Department of Civil and Environmental Engineering, Virginia Tech, Manassas, Virginia 20110, United States;* orcid.org/0000-0001-6221-7211; Email: stanleyg@vt.edu

Authors

Diver E. Marin − *Occoquan Watershed Monitoring Laboratory, Department of Civil and Environmental Engineering, Virginia Tech, Manassas, Virginia 20110, United States*

Shantanu V. Bhide − *Occoquan Watershed Monitoring Laboratory, Department of Civil and Environmental Engineering, Virginia Tech, Manassas, Virginia 20110, United States;* orcid.org/0000-0002-5248-0646

Megan A. Rippy − *Occoquan Watershed Monitoring Laboratory, Department of Civil and Environmental Engineering, Virginia Tech, Manassas, Virginia 20110, United States;* orcid.org/0000-0002-0575-8342

Jesus D. Gomez-Velez − *Environ. Sci. Division, Oak Ridge National Laboratory, Oak Ridge, Tennessee 37830, United States; Occoquan Watershed Monitoring Laboratory, Department of Civil and Environmental Engineering, Virginia Tech, Manassas, Virginia 20110, United States*

Robert N. Brent − *School of Integrated Sciences, James Madison University, Harrisonburg, Virginia 22807, United States*

Sujay S. Kaushal − *Department of Geology and Earth System Science Interdisciplinary Center, University of Maryland, College Park, Maryland 20742, United States*

Harold Post − *Occoquan Watershed Monitoring Laboratory, Department of Civil and Environmental Engineering, Virginia Tech, Manassas, Virginia 20110, United States*

Sydney Shelton − *Department of Geology and Earth System Science Interdisciplinary Center, University of Maryland, College Park, Maryland 20742, United States*

Shalini Misra − *School of Public and International Affairs, Virginia Tech, Arlington, Virginia 22203, United States*

Erin R. Hotchkiss − *Department of Biological Sciences, Virginia Tech, Blacksburg, Virginia 24061, United States*

Ahmed Monofy − *Occoquan Watershed Monitoring Laboratory, Department of Civil and Environmental Engineering, Virginia Tech, Manassas, Virginia 20110, United States*

Dongmei Alvi − *Occoquan Watershed Monitoring Laboratory, Department of Civil and Environmental Engineering, Virginia Tech, Manassas, Virginia 20110, United States*

Bradley Schmitz − *Loudoun Water, Ashburn, Virginia 20147, United States*

Shannon Curtis − *Fairfax County Public Works and Environmental Services, Fairfax, Virginia 22035, United States*

Christina C. Davis − *Loudoun Water, Ashburn, Virginia 20147, United States*

Peter Vikesland − *Dept. of Civil and Environ. Engineering, Virginia Tech, Blacksburg, Virginia 24061, United States;* orcid.org/0000-0003-2654-5132

Admin Husic − *Occoquan Watershed Monitoring Laboratory, Department of Civil and Environmental Engineering, Virginia Tech, Manassas, Virginia 20110, United States;* orcid.org/0000-0002-4225-2252

Complete contact information is available at: https://pubs.acs.org/10.1021/acs.est.5c04512

Notes

The authors declare no competing financial interest.

■ ACKNOWLEDGMENTS

This research was funded by an NSF Growing Convergence Research award (#2021015, 2020814, and 2312326). Additional support was provided by the Metropolitan Washington Council of Governments (MWCOG #21-001), Loudoun Water, VT's H2OStorm Initiative, the Watershed Dynamics and Evolution (WaDE) Science Focus Area at ORNL and ORNL SEED (11635) Tracking Disturbance Signals Along River Networks sponsored by the Laboratory Directed Research and Development Program of Oak Ridge National Laboratory, managed by UT-Battelle, LLC, for the U. S. Department of Energy.

REFERENCES

(1) Overbo, A.; Heger, S.; Gulliver, J. Evaluation of chloride contributions from major point and nonpoint sources in a northern U.S. state. *Sci. Total Environ.* **2021**, *764*, 144179.

(2) Kaushal, S. S.; Mayer, P. M.; Likens, G. E.; Reimer, J. E.; Maas, C. M.; Rippy, M. A.; Grant, S. B.; Hart, I.; Utz, R. M.; Shatkay, R. R.; Wessel, B. M.; Maietta, C. E.; Pace, M. L.; Duan, S.; Boger, W. L.; Yaculak, A. M.; Galella, J. G.; Wood, K. L.; Morel, C. J.; Nguyen, W.; Querubin, S. E. C.; Sukert, R. A.; Lowien, A.; Houde, A. W.; Roussel, A.; Houston, A. J.; Cacopardo, A.; Ho, C.; Talbot-Wendlandt, H.; Widmer, J. M.; Slagle, J.; Bader, J. A.; Chong, J. H.; Wollney, J.; Kim, J.; Shepherd, L.; Wilfong, M. T.; Houlihan, M.; Sedghi, N.; Butcher, R.; Chaudhary, S.; Becker, W. D. Five state factors control progressive stages of freshwater salinization syndrome. *Limnol. Oceanogr. Lett.* **2023**, *8*, 190−211.

(3) Kaushal, S. S.; Likens, G. E.; Mayer, P. M.; Shatkay, R. R.; Shelton, S. A.; Grant, S. B.; Utz, R. M.; Yaculak, A. M.; Maas, C. M.; Reimer, J. E.; Bhide, S. V.; Malin, J. T.; Rippy, M. A. The anthropogenic salt cycle. *Nat. Rev. Earth Environ.* **2023**, *4*, 770−784.

(4) Bhide, S. V.; Grant, S. B.; Parker, E. A.; Rippy, M. A.; Godrej, A. N.; Kaushal, S.; Prelewicz, G.; Saji, N.; Curtis, S.; Vikesland, P.; Maile-Moskowitz, A.; Edwards, M.; Lopez, K. G.; Birkland, T. A.; Schenk, T. Addressing the contribution of indirect potable reuse to inland freshwater salinization. *Nature Sustainability* **2021**, *4*, 699−707.

(5) Grant, S. B.; Rippy, M. A.; Birkland, T. A.; Schenk, T.; Rowles, K.; Misra, S.; Aminpour, P.; Kaushal, S.; Vikesland, P.; Berglund, E. Can common pool resource theory catalyze stakeholder-driven solutions to the freshwater salinization syndrome? *Environ. Sci. Technol.* **2022**, *56*, 13517−13527.

(6) Dugan, H. A.; Bartlett, S. L.; Burke, S. M.; Doubek, J. P.; Krivak-Tetley, F. E.; Skaff, N. K.; Summers, J. C.; Farrell, K. J.; McCullough, I. M.; Morales-Williams, A. M.; Roberts, D. C.; Ouyang, Z.; Scordo, F.; Hanson, P. C.; Weathers, K. C. Salting our freshwater lakes. *Proc. Natl. Acad. Sci. U. S. A.* **2017**, *114*, 4453−4458.

(7) Corsi, S. R.; De Cicco, L. A.; Lutz, M. A.; Hirsch, R. M. River chloride trends in snow-affected urban watersheds: increasing concentrations outpace urban growth rate and are common among all seasons. *Sci. Total Environ.* **2015**, *508*, 488−497.

(8) Kaushal, S. S.; Likens, G. E.; Pace, M. L.; Utz, R. M.; Haq, S.; Gorman, J.; Grese, M. Freshwater salinization syndrome on a continental scale. *Proc. Natl. Acad. Sci. U. S. A* **2018**, *115*, No. E574-E583.

(9) Stets, E. G.; Sprague, L. A.; Oelsner, G. P.; Johnson, H. M.; Murphy, J. C.; Ryberg, K.; Vecchia, A. V.; Zuellig, R. E.; Falcone, J. A.; Riskin, M. L. Landscape Drivers of Dynamic Change in Water Quality of U.S. Rivers. *Environ. Sci. Technol.* **2020**, *54*, 4336−4343.

(10) Kaushal, S. S.; Shelton, S. A.; Mayer, P. M.; Kellmayer, B.; Utz, R. M.; Reimer, J. E.; Baljunas, J.; Bhide, S. V.; Mon, A.; Rodriguez-Cardona, B. M.; Grant, S. B.; et al. Freshwater faces a warmer and saltier future from headwaters to coasts: climate risks, saltwater intrusion, and biogeochemical chain reactions. *Biogeochemistry* **2025**, *168*, 31.

(11) Reid, A. J.; Carlson, A. K.; Creed, I. F.; Eliason, E. J.; Gell, P. A.; Johnson, P. T.; Kidd, K. A.; MacCormack, T. J.; Olden, J. D.; Ormerod, S. J.; et al. Emerging threats and persistent conservation challenges for freshwater biodiversity. *Biol. Rev.* **2019**, *94*, 849−873.

(12) Van Gray, J. B.; Ayayee, P. Examining the impacts of salt specificity on freshwater microbial community and functional potential following salinization. *Environ. Microbiol.* **2024**, *26*, No. e16628.

(13) Szöcs, E.; Kefford, B. J.; Schäfer, R. B. Is there an interaction of the effects of salinity and pesticides on the community structure of macroinvertebrates? *Sci. Total Environ.* **2012**, *437*, 121−126.

(14) Cañedo-Argüelles, M.; Kefford, B. J.; Piscart, C.; Prat, N.; Schäfer, R. B.; Schulz, C.-J. Salinisation of rivers: An urgent ecological issue. *Environ. Pollut.* **2013**, *173*, 157−167.

(15) Brent, R. N.; Kunkel, J.; Tomek, Z.; Buchardt, D.; DeLisle, P. F.; Sivers, S. A Novel Approach to Developing Thresholds for Total Dissolved Solids Using Standardized and Experimental Toxicity Test Methods. *Environ. Toxicol. Chem.* **2022**, *41*, 2782−2796.

(16) DeVilbiss, S. E.; Badgley, B. D.; Hotchkiss, E. R.; Steele, M. K. Subsidy-stress responses of ecosystem functions along experimental freshwater salinity gradients. *Biogeochemistry* **2024**, *167*, 743−757.

(17) Kaushal, S. S.; Likens, G. E.; Pace, M. L.; Haq, S.; Wood, K. L.; Galella, J. G.; Morel, C.; Doody, T. R.; Wessel, B.; Kortelainen, P.; Räike, A.; Skinner, V.; Utz, R.; Jaworski, N. Novel 'chemical cocktails' in inland waters are a consequence of the freshwater salinization syndrome. *Philos. Trans. R. Soc., B* **2019**, *374*, 20180017.

(18) US Environmental Protection Agency publication *Ambient Water Quality Criteria for Chloride*; US Environmental Protection Agency publication, 1998.

(19) Cañedo-Argüelles, M.; Hawkins, C. P.; Kefford, B. J.; Schäfer, R. B.; Dyack, B. J.; Brucet, S.; Buchwalter, D.; Dunlop, J.; Frör, O.; Lazorchak, J.; et al. Saving freshwater from salts. *Science* **2016**, *351*, 914−916.

(20) Kaushal, S. S.; Wood, K. L.; Galella, J. G.; Gion, A. M.; Haq, S.; Goodling, P. J.; Haviland, K. A.; Reimer, J. E.; Morel, C. J.; Wessel, B. Making 'chemical cocktails'−Evolution of urban geochemical processes across the periodic table of elements. *Appl. Geochem.* **2020**, *119*, 104632.

(21) Hintz, W. D.; Fay, L.; Relyea, R. A. Road salts, human safety, and the rising salinity of our fresh waters. *Front. Ecol. Environ.* **2022**, *20*, 22−30.

(22) Shelton, S. A.; Kaushal, S. S.; Mayer, P. M.; Shatkay, R. R.; Rippy, M. A.; Grant, S. B.; Newcomer-Johnson, T. A. Salty chemical cocktails as water quality signatures: Longitudinal trends and breakpoints along different U.S. streams. *Sci. Total Environ.* **2024**, *930*, 172777.

(23) DewitzJon, U. G. S. *National Land Cover Database (NLCD) 2019 Products (ver. 2.0 June 2021)*; USGS, 2021.

(24) Blackburn, A. C. *Interpretive Guide to the use of Soils Maps of Loudoun County, Virginia*; Loudoun County Cooperative Extension Office, 1998.

(25) Horton, J. D. *The State Geologic Map Compilation (SGMC) Geodatabase of the Conterminous United States* (Accessed 30 May 2025). 2017; https://www.sciencebase.gov/catalog/item/5888bf4fe4b05ccb964bab9d.

(26) Han, Y.; Lau, S.-L.; Kayhanian, M.; Stenstrom, M. K. Characteristics of highway stormwater runoff. *Water Environ. Res.* **2006**, *78*, 2377−2388.

(27) Josse, J.; Husson, F. missMDA: a package for handling missing values in multivariate data analysis. *J. Stat. Soft.* **2016**, *70*, 1−31.

(28) Turnipseed, D. P.; Sauer, V. B. *Discharge Measurements At Gaging Stations*; USGS, 2010.

(29) Rets, E. P.; Kireeva, M. B.; Samsonov, T. E.; Ezerova, N. N.; Gorbarenko, A. V.; Frolova, N. L. Algorithm grwat for Automated Hydrograph Separation by B.I. Kudelin's Method: Problems and Perspectives. *Water Resour.* **2022**, *49*, 23−37.

(30) Li, L.; Maier, H. R.; Partington, D.; Lambert, M. F.; Simmons, C. T. Performance assessment and improvement of recursive digital baseflow filters for catchments with different physical characteristics and hydrological inputs. *Environ. Model. Softw.* **2014**, *54*, 39−52.

(31) Merz, R.; Parajka, J.; Blöschl, G. Time stability of catchment model parameters: Implications for climate impact analyses. *Water Resour. Res.* **2011**, *47*, W02531.

(32) Bergström, S. The development of a snow routine for the HBV-2 model. *Hydrol. Res.* **1975**, *6*, 73−92.

(33) Rosen, M. R.; Lapham, W. W. Introduction to the U.S. Geological Survey National Water-Quality Assessment (NAWQA) of Ground-Water Quality Trends and Comparison to Other National Programs. *J. Environ. Qual.* **2008**, *37*, S−190-S-198.

(34) Peres-Neto, P. R.; Jackson, D. A.; Somers, K. M. How many principal components? stopping rules for determining the number of non-trivial axes revisited. *Comput. Stat. Data Anal.* **2005**, *49*, 974−997.

(35) Rippy, M. A.; Deletic, A.; Black, J.; Aryal, R.; Lampard, J.-L.; Tang, J. Y.-M.; McCarthy, D.; Kolotelo, P.; Sidhu, J.; Gernjak, W.

Pesticide occurrence and spatio-temporal variability in urban run-off across Australia. *Water Res.* **2017**, *115*, 245−255.
(36) Le, S.; Josse, J.; Husson, F. FactoMineR: an R package for multivariate analysis. *J. Stat. Soft.* **2008**, *25*, 1−18.
(37) Skalski, J. R.; Richins, S. M.; Townsend, R. L. A statistical test and sample size recommendations for comparing community composition following PCA. *PLoS One* **2018**, *13*, No. e0206033.
(38) Davis, J. C.; Sampson, R. J. *Statistics and data analysis in geology*; Wiley New York, 1986; Vol. *646*.
(39) Cabin, R. J.; Mitchell, R. J. To Bonferroni or not to Bonferroni: when and how are the questions. *Bull. Ecol. Soc. Am.* **2000**, *81*, 246−248.
(40) Burton, J.; Gerritsen, J. *A Stream Condition Index for Virginia Non-Coastal Streams*; USEPA,2003.
(41) USDA *Virginia Department of Environmental Quality*; USDA, 2017.
(42) EPA *Causal Analysis/Diagnosis Decision Information System (CADDIS)*. https://www.epa.gov/caddis, 2017;(Accessed 30 May 2025).
(43) Hrachowitz, M.; Benettin, P.; Van Breukelen, B. M.; Fovet, O.; Howden, N. J.; Ruiz, L.; Van Der Velde, Y.; Wade, A. J. Transit times-the link between hydrology and water quality at the catchment scale. *Wires Water* **2016**, *3*, 629−657.
(44) Norrström, A. C.; Bergstedt, E. *The Impact of Road De-Icing Salts (NaCl) on Colloid Dispersion and Base Cation Pools in Roadside Soil*; Springer, 2001.
(45) Price, J. R.; Szymanski, D. W. The effects of road salt on stream water chemistry in two small forested watersheds, Catoctin Mountain, Maryland, USA. *Aquat. Geochem.* **2014**, *20*, 243−265.
(46) Larson, J. D. *Chemical composition of streams during low flow; Fairfax County*; United States Geological Survey: Virginia, 1978.
(47) Mazumder, B.; Wellen, C.; Kaltenecker, G.; Sorichetti, R. J.; Oswald, C. J. Trends and legacy of freshwater salinization: untangling over 50 years of stream chloride monitoring. *Environ. Res. Lett.* **2021**, *16*, 095001.
(48) Flydulles.com *Washington's Airports Set New Passenger Record* (Accessed 6 March 2025). https://www.flydulles.com/news/washingtons-airports-set-new-passenger-record.
(49) Federal Aviation Administration *Advisory Circular 150/5200−30D, Change 2: airport Winter Safety And operationsadvisory Circular*; Federal Aviation Administration, 2020.
(50) Evans, M.; Frick, C. *Effects Of Road Salts On Aquatic Ecosystems*; Stoney Creek Environment Committee, **2001**.
(51) Miller, J. R.; LaLama, M. J.; Kusnic, R. L.; Wilson, D. E.; Kiraly, P. M.; Dickson, S. W.; Zeller, M. On the nature of calcium magnesium acetate road deicer. *J. Solid State Chem.* **2019**, *270*, 1−10.
(52) Froelich, A.; Zenone, C. *The Relation of Water Quality to Geology and Land Use Changes in Fairfax County and Vicinity*; Virginia, 1985.
(53) Webber, J. S.; Chanat, J. G.; Porter, A. J.; Jastram, J. D. *Evaluating Drivers of Hydrology, Water Quality, and Benthic Macroinvertebrates in Streams of Fairfax County, Virginia, 2007−18*; Virginia, 2023.
(54) Posner, A.; Zenone, C. *Chemical Quality of Ground Water in the Culpeper Basin*; Virginia, 1983.
(55) Dinar, A.; Quinn, N. W. Developing a decision support system for regional agricultural nonpoint salinity pollution management: application to the San Joaquin River, California. *Water* **2022**, *14*, 2384.
(56) Borah, D. K.; Zhang, H. X.; Zellner, M.; Ahmadisharaf, E.; Babbar-Sebens, M.; Quinn, N. W. T.; Kumar, S.; Sridharan, V. K.; Leelaruban, N.; Lott, C.; et al. Advances in Total Maximum Daily Load Implementation Planning by Modeling Best Management Practices and Green Infrastructures. *J. Environ. Eng.* **2024**, *150*, 03124003.
(57) Askarizadeh, A.; Rippy, M. A.; Fletcher, T. D.; Feldman, D. L.; Peng, J.; Bowler, P.; Mehring, A. S.; Winfrey, B. K.; Vrugt, J. A.; AghaKouchak, A.; Jiang, S. C.; Sanders, B. F.; Levin, L. A.; Taylor, S.; Grant, S. B. From Rain Tanks to Catchments: Use of Low-Impact Development To Address Hydrologic Symptoms of the Urban Stream Syndrome. *Environ. Sci. Technol.* **2015**, *49*, 11264−11280.
(58) Pond, G. J. Biodiversity Loss in Appalachian Headwater Streams (Kentucky, USA): Plecoptera and Trichoptera Communities. *Hydrobiologia* **2012**, *679*, 97−117.
(59) Pond, G. J. Patterns of Ephemeroptera Taxa Loss in Appalachian Headwater Streams (Kentucky, USA). *Hydrobiologia* **2010**, *641*, 185−201.
(60) Jastram, J. D. *Streamflow, Water Quality, and Aquatic Macroinvertebrates of Selected Streams in Fairfax County*; Virginia, 2014.
(61) Virginia *Volume I Stressor Analysis Report for the Benthic Macroinvertebrate Impairments in the Accotink Creek Watershed, Fairfax County*; Virginia. 2017.
(62) Virginia. *Integrated Report*; Virginia, 2024
(63) Appendix 1b Supplemental List of Category 5 Waters Newly Impaired in 2024 (303(d) List).
(64) Schuler, M. S.; Cañedo-Argüelles, M.; Hintz, W. D.; Dyack, B.; Birk, S.; Relyea, R. A. Regulations are needed to protect freshwater ecosystems from salinization. *Philos. Trans. R. Soc., B* **2019**, *374*, 20180019.
(65) Yang, Y.-Y.; Toor, G. S. Sources and mechanisms of nitrate and orthophosphate transport in urban stormwater runoff from residential catchments. *Water Res.* **2017**, *112*, 176−184.
(66) Kaushal, S. S.; Maas, C. M.; Mayer, P. M.; Newcomer-Johnson, T. A.; Grant, S. B.; Rippy, M. A.; Shatkay, R. R.; Leathers, J.; Gold, A. J.; et al. Longitudinal stream synoptic monitoring tracks chemicals along watershed continuums: a typology of trends. *Front. Environ. Sci.* **2023**, *11*, 1122485.
(67) Maas, C. M.; Kaushal, S. S.; Rippy, M. A.; Mayer, P. M.; Grant, S. B.; Shatkay, R. R.; Malin, J. T.; Bhide, S. V.; Vikesland, P.; Krauss, L.; et al. Freshwater salinization syndrome limits management efforts to improve water quality. *Front. Environ. Sci.* **2023**, *11*, 1106581.
(68) Booth, D. B.; Jackson, C. R. URBANIZATION OF AQUATIC SYSTEMS: DEGRADATION THRESHOLDS, STORMWATER DETECTION, AND THE LIMITS OF MITIGATIO[1]. *JAWRA* **1997**, *33*, 1077−1090.
(69) Hogan, D. M.; Walbridge, M. R. Best Management Practices for Nutrient and Sediment Retention in Urban Stormwater Runoff. *J. Environ. Qual.* **2007**, *36*, 386−395.
(70) Rugh, M. B.; Grant, S. B.; Hung, W.-C.; Jay, J. A.; Parker, E. A.; Feraud, M.; Li, D.; Avasarala, S.; Holden, P. A.; Liu, H.; Rippy, M. A.; Werfhorst, L. C. V. D.; Kefela, T.; Peng, J.; Shao, S.; Graham, K. E.; Boehm, A. B.; Choi, S.; Mohanty, S. K.; Cao, Y. Highly variable removal of pathogens, antibiotic resistance genes, conventional fecal indicators and human-associated fecal source markers in a pilot-scale stormwater biofilter operated under realistic stormflow conditions. *Water Res.* **2022**, *219*, 118525.
(71) Parker, E. A.; Grant, S. B.; Sahin, A.; Vrugt, J. A.; Brand, M. W. Can smart stormwater systems outsmart the weather? Stormwater capture with real-time control in southern California. *ACS EST Water* **2022**, *2*, 10−21.
(72) Kaushal, S. S.; Reimer, J. E.; Mayer, P. M.; Shatkay, R. R.; Maas, C. M.; Nguyen, W. D.; Boger, W. L.; Yaculak, A. M.; Doody, T. R.; Pennino, M. J.; et al. Freshwater salinization syndrome alters retention and release of chemical cocktails along flowpaths: From stormwater management to urban streams. *Freshw. Sci.* **2022**, *41*, 420−441.
(73) Galella, J. G.; Kaushal, S. S.; Mayer, P. M.; Maas, C. M.; Shatkay, R. R.; Stutzke, R. A. Stormwater best management practices: Experimental evaluation of chemical cocktails mobilized by freshwater salinization syndrome. *Front. Environ. Sci.* **2023**, *11*, 1020914.
(74) Long, S.; Rippy, M. A.; Krauss, L.; Stacey, M.; Fausey, K. The impact of deicer and anti-icer use on plant communities in stormwater detention basins: Characterizing salt stress and phytoremediation potential. *Sci. Total Environ.* **2025**, *962*, 178310.
(75) Galella, J. G.; Kaushal, S. S.; Wood, K. L.; Reimer, J. E.; Mayer, P. M. Sensors track mobilization of 'chemical cocktails' in streams impacted by road salts in the Chesapeake Bay watershed. *Environ. Res. Lett.* **2021**, *16*, 035017.

(76) Moore, J.; Fanelli, R. M.; Sekellick, A. J. High-Frequency Data Reveal Deicing Salts Drive Elevated Specific Conductance and Chloride along with Pervasive and Frequent Exceedances of the U.S. Environmental Protection Agency Aquatic Life Criteria for Chloride in Urban Streams. *Environ. Sci. Technol.* **2020**, *54*, 778−789.
(77) Pellerin, B. A.; Saraceno, J. F.; Shanley, J. B.; Sebestyen, S. D.; Aiken, G. R.; Wollheim, W. M.; Bergamaschi, B. A. Taking the Pulse of Snowmelt: In Situ Sensors Reveal Seasonal, Event and Diurnal Patterns of Nitrate and Dissolved Organic Matter Variability in an Upland Forest Stream. *Biogeochemistry* **2012**, *108*, 183−198.
(78) Fay, L.; Shi, X. Environmental Impacts of Chemicals for Snow and Ice Control: State of the Knowledge. *Water, Air, Soil Pollut.* **2012**, *223*, 2751−2770.
(79) Monks, A. M.; Lishawa, S. C.; Ohsowski, B. M.; Schurkamp, S. J.; Lawrence, B. A. Complementarity of road salt and heavy metal pollutant removal through invasive Typha and Phragmites harvest in urban wetland detention basins. *Ecol. Eng.* **2023**, *194*, 107058.

https://doi.org/10.1021/acs.est.5c04512
Environ. Sci. Technol. 2025, 59, 14053−14062

Supporting Information for *Ion Clusters Reveal the Sources, Impacts, and Drivers of Freshwater Salinization*

Diver E. Marin, Stanley B. Grant,* Shantanu V. Bhide, Megan A. Rippy, Jesus D. Gomez-Velez, Robert N. Brent, Sujay S. Kaushal, Harold Post, Sydney Shelton, Shalini Misra, Erin R. Hotchkiss, Ahmed Monofy, Dongmei Alvi, Bradley Schmitz, Shannon Curtis, Christina C. Davis, Peter Vikesland, and Admin Husic

E-mail: stanleyg@vt.edu

Summary of content: 20 pages, 6 tables and 11 figures

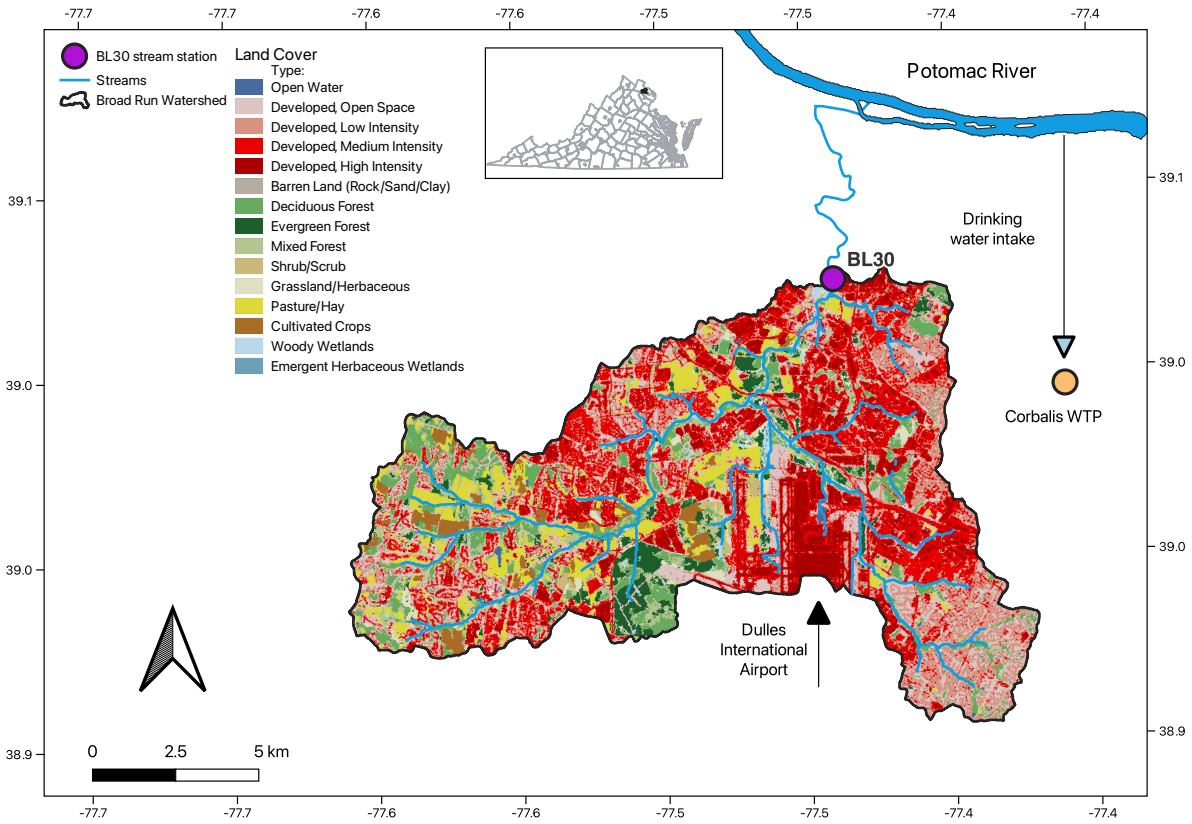

Figure S1: Broad Run drains a highly urbanized 152 km^2 portion of Loudoun County, Northern Virginia, USA (shown in the inset map). Our 3-year study analyzes hydrology and water quality measurements at stream station BL30 (39.024°N, 77.439°W), shown as a purple filled circle at the north-central edge of the delineated drainage. The Washington Dulles International Airport, which serves over 24 million travelers per year, is visible in the south-central portion of the drainage. The orange circle is the approximate location of the Corbalis drinking water treatment plant, which serves a population of over 1 million people. The Corbalis raw water intake is located approximately 10 km downstream of the confluence of Broad Run and the Potomac River.

Table S1: Land cover types in the portion of the Broad Run watershed that drains to BL30.

Cover type	**Area (km^2)**	**Percentage (%)**
Developed, Medium Intensity	34.2	22.4
Developed, Low Intensity	28.7	18.8
Developed, Open Space	20.6	13.5
Developed, High Intensity	16.8	11.0
Deciduous Forest	14.0	9.21
Pasture/Hay	12.6	8.28
Mixed Forest	8.19	5.37
Evergreen Forest	6.33	4.15
Cultivated Crops	4.06	2.66
Grassland/Herbaceous	2.60	1.71
Woody Wetlands	1.97	1.29
Shrub/Scrub	1.25	0.818
Open Water	0.473	0.311
Barren Land	0.428	0.281
Emergent Herbaceous Wetlands	0.192	0.126

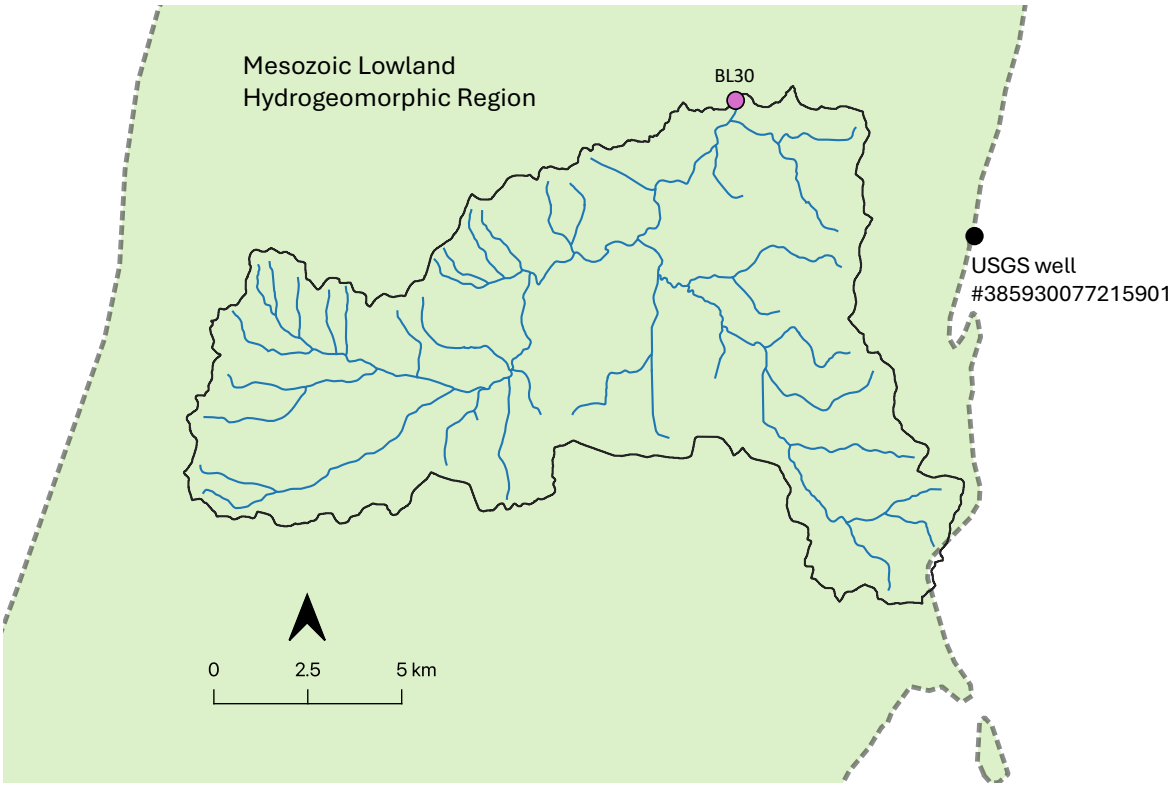

Figure S2: The location of the USGS groundwater well, relative to the BL30 monitoring station on Broad Run. The groundwater well and BL30 drainage area are located within the Mesozoic Lowland (Triassic Basin) hydrogeomorphic region of Virginia.

Note S1: Watershed LULC and Geology

Land Use and Land Cover data were retrieved from the National Land Cover Dataset[1] and are shown in Figure S1 and summarized in Tables S1 and S2. The watershed lies within Virginia's Mesozoic Lowland Hydrogeomorphic Region, which is underlain primarily by siltstone, shale, sandstone, diabase and basalt rock types (Figures S2 and S3).

Table S2: Grouped land cover types within Broad Run watershed.

Cover type	Area (km^2)	Percentage
Developed	100.25	65.78
Forest	28.54	18.73
Cultivated	16.67	10.94
Grassland/Herbaceous	2.60	1.70
Wetlands	2.16	1.41
Shrub/Scrub	1.24	0.81
Open water	0.47	0.31
Barren land	0.42	0.28

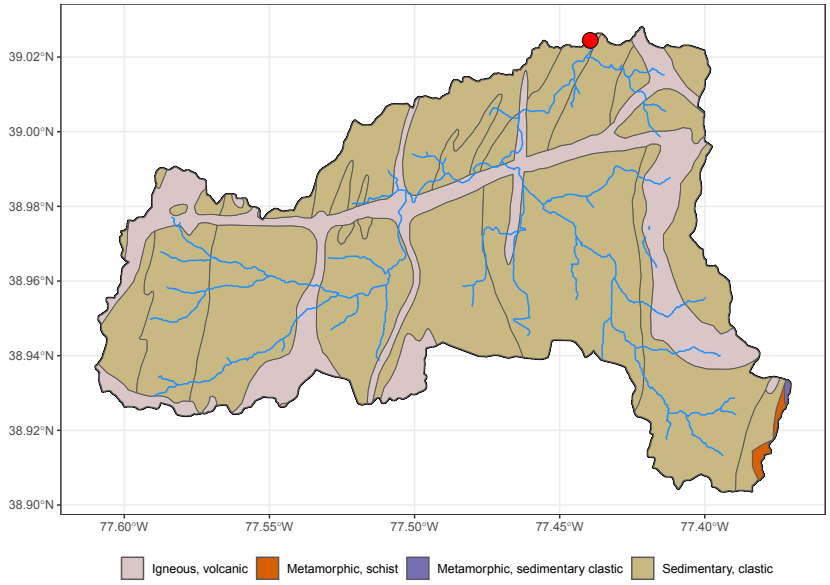

Figure S3: Geology outcrops within the portion of the Broad Run watershed that drains to BL30.[2]

Note S2: Sample Collection and Field Measurements

Water samples were collected from station BL30 during baseflow and storm events as follows.

Base Flow Sampling. Baseflow grab samples were collected every other week during dry weather periods. During each baseflow sampling event, two grab samples were collected from the stream, one for dissolved ions and another for nutrient analysis. The grab sample for dissolved ions was filtered in the field through a 0.45 micron syringe filter (Filtrous Lab, 30 mm GFP filters). Stream water temperature, specific conductance, and pH were measured onsite with a multimeter (YSI Multimeter, ProDSS), which was calibrated prior to each sampling event. Stream water total alkalinity was measured onsite by sulfuric acid titration (Hach Digital Titrator). Field measurements of pH and total alkalinity were used to estimate bicarbonate concentration in each sample (HCO_3^-)[3] (see Note S4). For safety reasons, no field measurements were conducted during storm events. All samples were transported to the Occoquan Watershed Monitoring Laboratory on ice within 4 h for further processing. A total of 79 baseflow samples were collected and analyzed over the three-year study.

Storm Flow Samples. Automated flow-weighted composite samples of storm events were triggered when the rate of increase in stream stage exceeded 3.3×10^{-5} feet per minute. Once triggered, a Manning Portable Vacuum Sampler (Model VST3a) was programmed to accumulate 200 mL of sample volume for every 1 million cubic feet of stream flow. For safety reasons no onsite measurements (e.g., for pH, temperature, specific conductance, or total alkalinity, see above) were collected during storm sampling events. Composite samples were transported to the Occoquan Watershed Monitoring Laboratory on ice within one day following the end of a storm. At the lab, 25 mL of the composite sample was filtered through a 0.45 micron syringe filter (Filtrous Lab, 30 mm GFP filters) for dissolved ion analysis. A total of 74 storm samples were collected over the three-year study.

Note S3: Laboratory Analysis

Within 1 day of arriving at the lab, the pre-filtered baseflow and storm samples (see above) were analyzed for dissolved ions (K^+, Na^+, Cl^-, SO_4^{2-}, Ca^{2+}, Mg^{2+}) using ion chromatography (Dionex, ICS 5000) following ASTM D6919-09 and Standard Method 4110 B-2011.

The unfiltered baseflow and storm samples were analyzed for total and dissolved nutrients as follows.

For total nutrients, 10 mL unfiltered sample was immediately persulfate digested, stored at 4°C, and analyzed within 28 days for total nitrogen (TN, the sum of dissolved inorganic N, dissolved organic N, and particulate N species) and total phosphorus (TP, the sum of dissolved inorganic phosphorus, dissolved organic phosphorus, and particulate phosphorus) using an Astoria Pacific Model 411S Autoanalyzer with a 307 Detector (Standard Method 4500-P J-2011).

For dissolved nutrients, immediately upon arrival at the lab, approximately 200 mL of the unfiltered field sample was filtered through glass microfiber filters (Whatman, 934-AH). The filtrate was stored at -20°C and, within 28 days of arrival, analyzed for dissolved nitrate plus nitrite (NO_3^-/NO_2^- =NO_3^- + NO_2^-) and orthophosphate (PO_4^{-3}) using an Astoria Pacific, Model 311 Autoanalyzer with a 305D Detector (Standard Methods 4500-NO3- F-2011, 4500-P F-2011).

All analyses were conducted in accordance with the Occoquan Watershed Monitoring Laboratory's Virginia Environmental Laboratory Accreditation Program (VELAP #460026). The lower-limit of detection (LOD) for each analyte is indicated in Table S3.

Table S3: List of constituents measured in this study and associated LODs.

Chemical measures	**Units**	**Limit of detection**
Chloride	mg/L	5.0 mg/L
Magnesium	mg/L	0.5 mg/L
Calcium	mg/L	1.5 mg/L
Sulfate	mg/L	5.0 mg/L
Bicarbonate	NA	NA
Sodium	mg/L	1.5 mg/L
Potassium	mg/L	1.0 mg/L
Total Alkalinity	mg/L as $CaCO_3$	0.1 mg/L as $CaCO_3$
Total Phosphorus	mg/L	0.01 mg/L
Total Nitrogen	mg/L	0.25 mg/L
Specific Conductance	μS/cm	NA
Dissolved Orthophosphate	mg/L	0.01 mg/L
Ammonium	mg/L	0.01 mg/L
Oxidized Nitrogen Species	mg/L	0.01 mg/L

Note S4: Bicarbonate Ion Concentrations

Bicarbonate ion concentrations were estimated using two different approaches, one approach for baseflow samples and another for storm samples. Bicarbonate concentrations in baseflow samples were estimated directly from measured total alkalinity expressed in units of mg/L as $CaCO_3$; over the pH range (6.7 to 8.1) measured in baseflow samples, most of the total alkalinity is in the form of bicarbonate. However, this approach could not be used to estimate bicarbonate ion concentrations in storm samples, because safety concerns precluded field measurements of total alkalinity during storms (see Note S2).

Instead, bicarbonate ion concentrations in storm samples were imputed using a regularized iterative PCA method that identifies dominant water quality patterns across the entire dataset (baseflow + storm samples, $N = 153$) and "fills in" missing values based on the dominant patterns identified (see Methods Section in the main text for details). By this approach, missing bicarbonate ion concentrations were imputed for all 74 storm samples.

The accuracy of the imputed bicarbonate concentrations was checked in two ways: (1) by assessing the charge balance error (CBE) associated with measured and imputed ion

concentrations in each storm sample (see Note S5); and (2) by comparing to bicarbonate concentrations estimated using a geochemical approach, in which all unbalanced (anionic) charge is attributed to bicarbonate. Bicarbonate concentrations estimated by the latter approach are highly correlated with bicarbonate concentrations estimated by the regularized iterative PCA method (Pearson Correlation, R =0.84) and fall close to, but consistently above (PBIAS=13.8%), the 1:1 line (Figure S4); note that the outlier in the cross-plot corresponds to a sample that was ultimately removed (i.e., not included in subsequent analyses) because it did not meet the requirement that absolute value of the CBE should be less than 10% (see Note S5).

This result—that bicarbonate concentrations estimated by charge balance are strongly correlated but biased high relative to bicarbonate concentrations estimated by the regularized

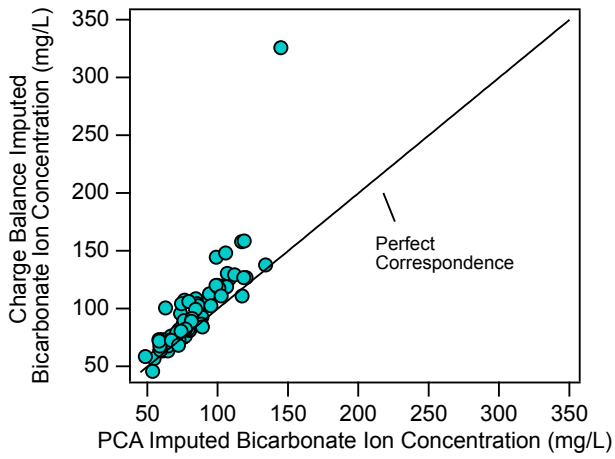

Figure S4: A comparison of bicarbonate concentrations imputed for storm samples based on either charge balance (vertical axis) or regularized iterative PCA (horizontal axis). The bicarbonate concentrations estimated by these two approaches are highly correlated, although values estimated using the geochemical approach are consistently biased high, likely due to the presence of unquantified organic acids in the storm samples.

Note S5. Electroneutrality analysis

The measured and imputed ion concentrations in each baseflow and storm sample were checked for overall electroneutrality. Specifically, we calculated a Charge Balance Error (CBE) based on the normality, N, of all measured or imputed cations (H^+, K^+, Na^+, Ca^{2+}, Mg^{2+}, NH_4^+) and anions (HCO_3^-, Cl^-, SO_4^{2-},NO_3^-/NO_2^-, PO_4^{3-}):

$$CBE(\%) = \frac{\sum N_{cation,i} - \sum N_{anion,i}}{\sum N_{cation,i} + \sum N_{anion,i}} * 100 \quad (1)$$

Of the 153 baseflow and storm samples screened, only four (two baseflow and two storm samples) had an absolute CBE greater than 10%, a generally accepted criterion for assessing electroneutrality of ion measurements in low-ionic-strength surface waters.[4] The fact that all but two storm samples conformed to this electroneutrality criterion lends credibility to the bicarbonate concentrations imputed for all storm samples (see Note S4). The four samples with absolute CBE >10% were excluded from further analysis (i.e., they were not included in the PCA and clustering steps). The CBE for the retained 77 baseflow samples ranged from −4.37% to 6.23%, while the CBE for the retained 72 storm samples ranged from −4.2% to 7.01% (Figure S5).[4]

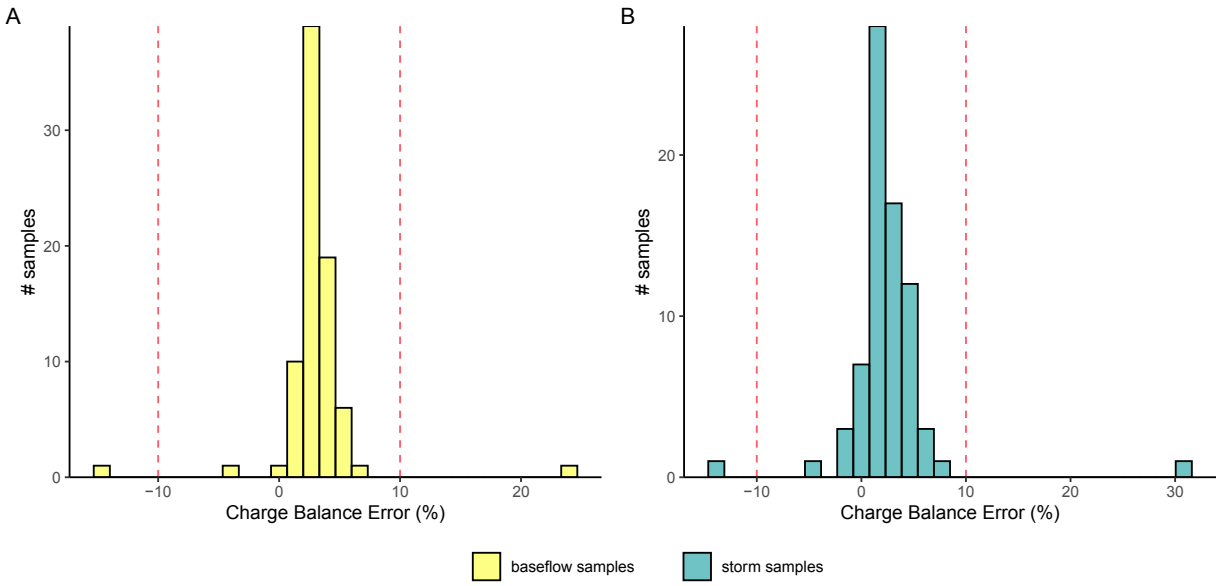

Figure S5: Charge Balance Error (CBE) calculated based on measured or imputed ion concentrations in each baseflow (left histogram) or storm (right histogram) sample. The vertical dashed red lines denote the ±10% CBE criteria typically applied to ion measurements in low ionic strength surface waters like Broad Run.

Note S6: Environmental Data

The sources of environmental data are summarized in Table S4, while the data themselves are plotted as a time series in Figure S6 and described in more detail below.

Table S4: Environmental data included in this study

Variable	Time period	Source
Streamflow	2010-2023	OWML
Precipitation	2010-2023	NOAA
Temperature	2010-2023	NOAA
Rainfall	2010-2023	HBV model
Snowmelt	2010-2023	HBV model

Stream Discharge. Stream discharge was measured at station BL30 at an hourly time step by the Occoquan Watershed Monitoring Laboratory (OWML) from 2020 to 2023. These hourly discharge data were averaged to a daily time step for further analysis. Continuous

discharge data were missing on only five days, due to routine maintenance of the gauge at BL30: 2020-06-10, 2021-01-21, 2021-05-26, 2022-06-13 and 2023-02-12. These one-day long data gaps were filled using linear interpolation (zoo package in R).[5]

Precipitation. Daily precipitation measured at the Washington Dulles International Airport station was retrieved from NOAA. For input to the HBV model (Note S8), these daily data were extrapolated to an hourly time step using the persistence model. Trace measurements of precipitation were taken as equal to zero.

Air Temperature. Daily air temperature measured at the Washington Dulles International Aiport weather station was retrieved from NOAA, including daily average, minimum and maximum temperatures. For input to the HBV model (described below), these daily data were converted to an hourly time step using the package ChillR in R,[6] which generates hourly temperature records for a particular location based on minimum and maximum daily temperature, along with the location's latitude.

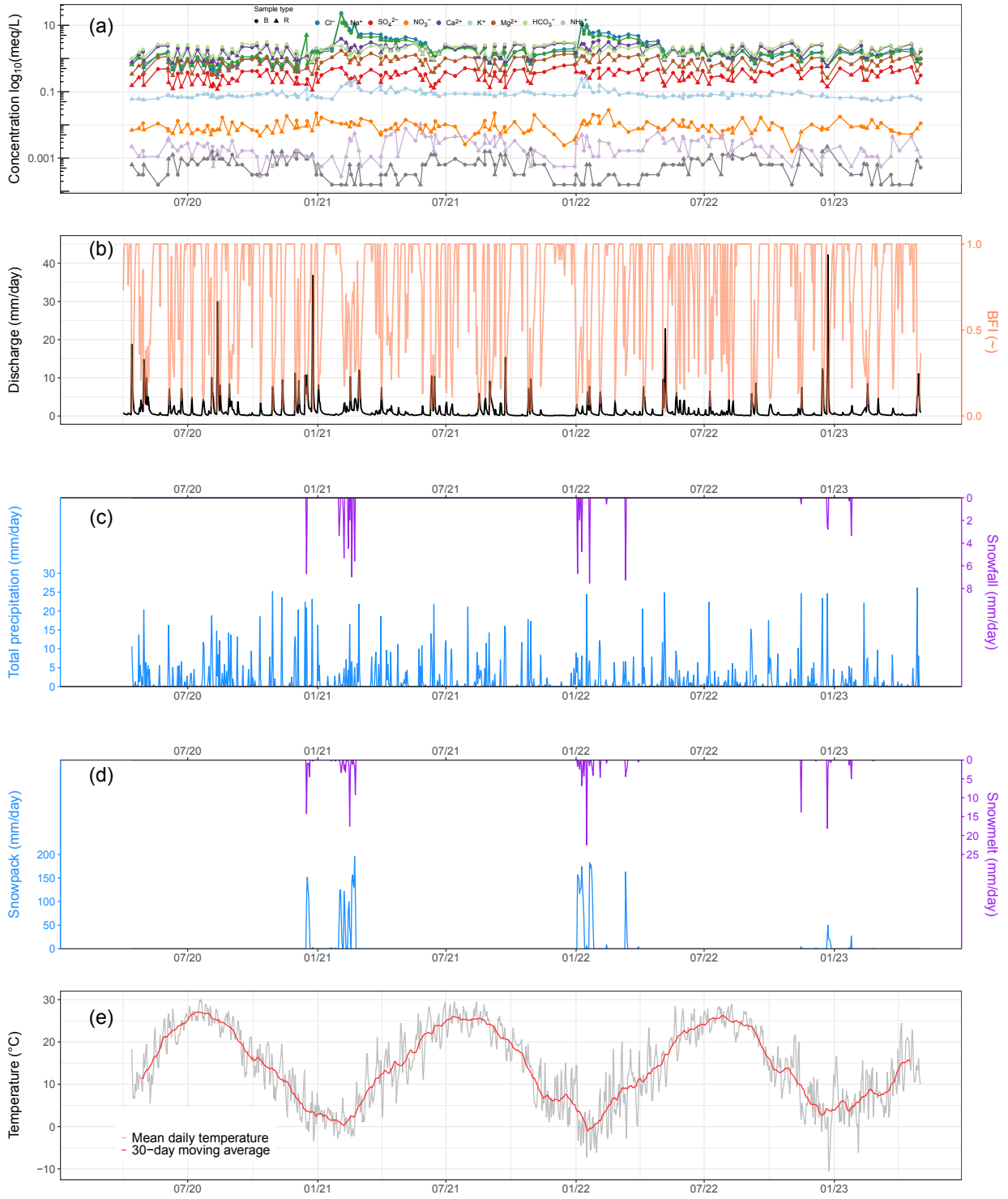

Figure S6: Daily timeseries of: a) ion measurements (Ca^{2+}, Mg^{2+}, NH_4^+, K^+, Na^+, Cl^-, SO_4^{2-}, NO_3^-/NO_2^-, HCO_3^-) in baseflow and stormflow samples; b) snowmelt and rainfall; c) discharge and BFI; and d) air temperature.

Note S7: Baseflow Index (BFI)

To estimate base flow we applied a Recursive Digital Filter (RDF) to the stream discharge measurements at BL30. The RDF method isolates the high-frequency (i.e., quick flow) and low-frequency (i.e., base flow) signals from the stream discharge hydrograph using a digital filter.[7] For these calculations we used the grwat package in R, and adopted the Lyne and Hollick (LH) digital filter as follows:

$$q_{f(i)} = aq_{i-1} + \frac{1+\alpha}{2}(q_i - q(i-1)); q_{f(i)\geq 0} \tag{2}$$

$$q_{b(i)} = q_i - q_{f(i)} \tag{3}$$

Here, the subscript i is the time step, q_i is the total streamflow at time step i, $q_{f(i)}$ and $q_{b(i)}$ are the filter quickflow and baseflow at time step i, and a is a dimensionless filter parameter which can vary from. $a \in \{0, 1\}$.[7] For our analysis we adopted the value $a = 0.925$ as recommended by Zhang et al.[8] Base Flow Index (BFI) was then computed from the ratio of the estimated baseflow and measured streamflow. Measured stream flow at BL30 is compared with baseflow estimates in Figure S7.

Note S8: Hydrologiska Byråns Vattenbalansavdelning (HBV) Model Estimates of Snowmelt

The HBV model is a rainfall-runoff model with routines for different components of the water cycle (e.g., snow routine, soil routine, groundwater routine for response and routing, etc.)[9] The snow routine of the HBV model was used to capture (1) the partitioning of precipitation, $P(t)$, between rainfall, $r(t)$, and snowfall, and (2) the accumulation of snowpack and generation of snow melt, $s(t)$. Model parameters include (1) the threshold temperature, T_T

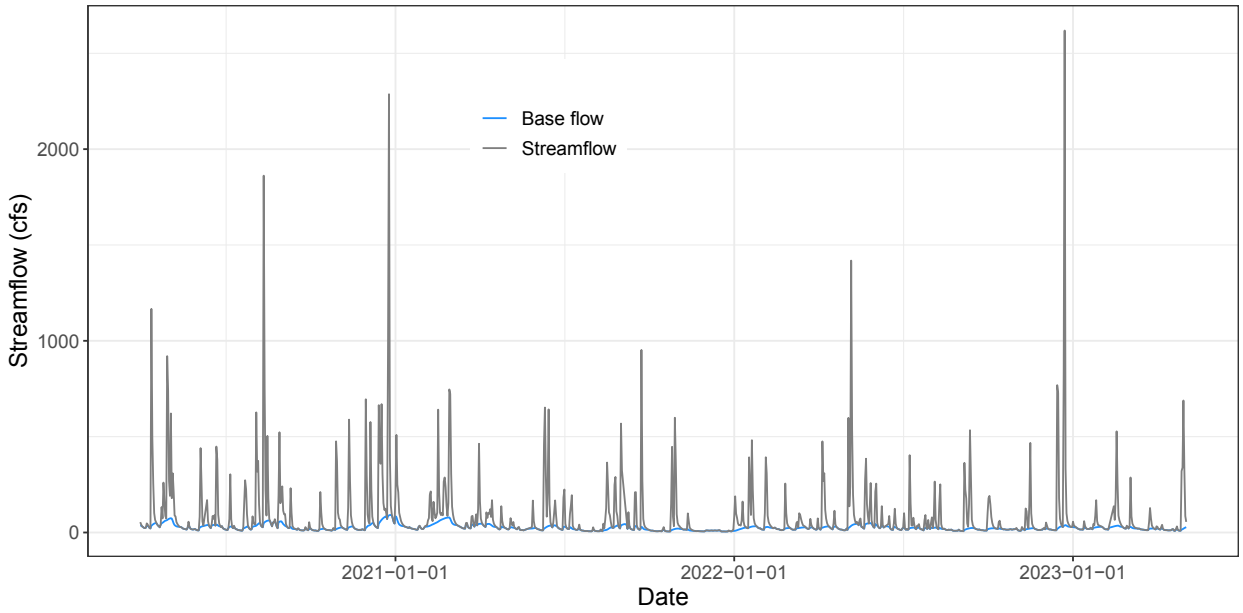

Figure S7: Measured streamflow at BL30 station compared to base flow estimated using a recursive digital filter. For the recursive filter we adopted the Lyne and Hollick method with $a = 0.925$.

(in °K), below which all precipitation is considered to fall as snow, (2) the snowfall correction factor, SF_{cf}, which accounts for snowfall undercatch due to wind turbulence, catchment vegetation, and other factors,[10,11] (3) the degree-day factor, D_F, which is a proportionality constant for estimating snow melt, (4) the water holding capacity of the snowpack, W_H, and (5) the refreezing coefficient, F, which allows for refreezing of the melted water when air temperature, $T_{air}(t)$ (in °K), falls below T_T. Model parameters for snow accumulation were selected to represent weather conditions in the Mid-Atlantic region of the United States (Table S5). Accumulated snow depth at Dulles International Airport, downloaded from the NOAA website (www.ncei.noaa.gov), was used to verify that the timing of HBV model-predicted snow melt events aligned with the date of zero accumulated snow depth reported at Dulles Airport after snow events. From these comparisons, we estimated that the HBV snow model accurately predicts snow melt at Dulles roughly 83% of the time.

Table S5: HBV model parameters.

Parameter	Value
T_T	0° C
SF_{cf}	1.1
D_F	7.29×10^{-5} m °C^{-1} h^{-1}
W_H	0.1
F	0.05

Note S9: Resampling-Based Approach for Identifying Significant Principal Components

A resampling-based stopping rule was used to identify the principal components (PCs) that explained significantly more variance in the ions measurements than would be expected by chance (at the 95% confidence level) (Figure S8). The method was implemented as follows:[12] 1) Principal Component Analysis (PCA) was performed on log-transformed and Z-scored data and the eigenvalues for each principal component were saved (EIGdata); 2) Variables in the data matrix were randomized 10,000 times; 3) PCA was conducted on these randomized matrices and the eigenvalues for each principal component were saved (EIGrand); 4) percentile-based 95% confidence intervals were calculated for each principal component using the generated EIGrand values (10,000 realizations per mode); 5) PCs for which EIGdata exceeded $\geq$ the 95th percentile value of EIGrand were determined to be significant and retained as dominant dimensions.

Note S10. Benthic Community Response Thresholds

The VDEQ state-wide ion thresholds and probability monitoring data described in the main text were compared to ion and nutrient measurements at BL30 as follows (see also[13]): (1) VDEQ's probability monitoring dataset was filtered to include only sites in the Northern Piedmont Ecoregion where BL30 is located; (2) A set of cumulative distribution functions

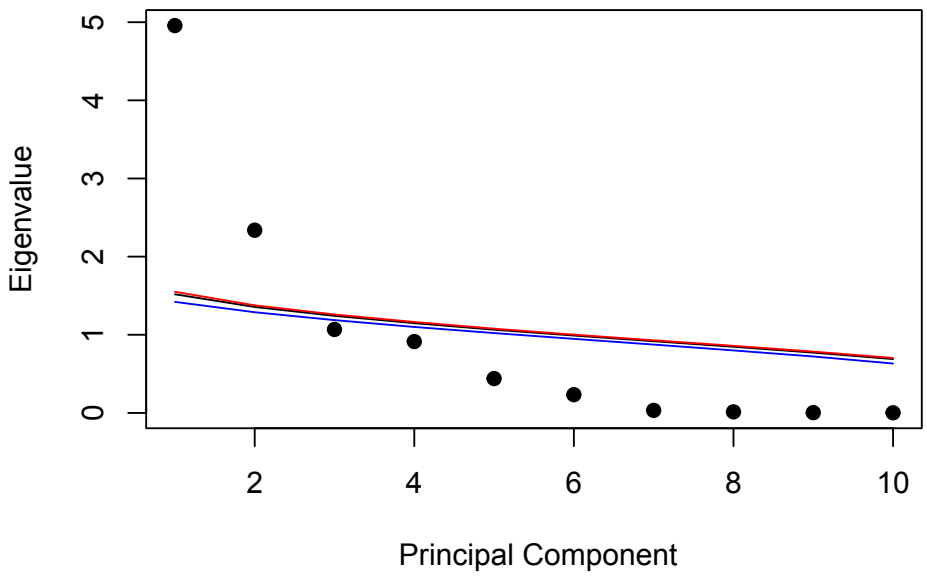

Figure S8: Principal components (x-axis) and associated eigenvalues (y-axis) for the PCA analysis conducted in this study. Also shown are the resampling-based stopping rule estimates for the eigenvalues expected by chance for a random threshold of 95%, 90%, and %50 (red, black, and blue lines, respectively). PC1 and PC2 exceed the upper 95% confidence threshold (red line) implying that they these two principal components are significant at a $p \leq 0.05$.

(CDFs) (one for each ion and nutrient) were prepared for VDEQ's stream ion and nutrient measurements in the Northern Piedmont Ecoregion; (3) using the CDFs from (2), each ion and nutrient measurement at BL30 was converted into a corresponding non-exceedance probabilities (i.e., the percentage of stream sites in the Northern Piedmont Ecoregion with that concentration or lower); and (4) results from (3) were combined with VDEQ's state-wide benthic community response thresholds, to estimate probable impact on aquatic life.

Note S11. Ion Slopes

The salt ion concentrations measured in an urban stream likely reflect a time-varying mixture of various watershed salt sources, each with its own set of potentially unique ion ratios, along with myriad biogeochemical reactions that occur as the ions transport along flow paths through the watershed.[14] The overprinting of multiple sources and biogeochemical processes implies that ion ratios measured in the stream are unlikely to have much diagnostic value.

On the other hand, if a particular source is driving sample-to-sample variability in measured salinity, its ion ratio might manifest as a consistent molar increase in one ion relative to another; i.e., the slope obtained when the molar concentrations of the two ions are cross-plotted. For example, at BL30 we might predict that an increase in the molar concentration of sodium, ΔNa^+ (where the symbol Δ denotes increase), is associated with a near equal increase in the molar concentration of chloride, ΔCl^-, given the dominant use of NaCl (in either its crystalline or brine forms) for road and parking lot deicers and anti-icers.[15]

To test this idea, we cross-plotted the molar concentrations of ion pairs commonly associated with deicers (Figure S9) and geogenic sources (Figure S10). The deicers evaluated included NaCl (Figure S9a), $CaCl_2$ (Figure S9b), $MgCl_2$ (Figure S9c), and magnesium calcium acetate ($Mg_2Ca(OAc)_6$) (Figure S9d). Geogenic sources are assumed to lead to correlated increases in the molar concentrations of magnesium and sulfate (Figure S10a), calcium and sulfate (Figure S10b), magnesium and bicarbonate (Figure S10c), and calcium

and bicarbonate (Figure S10d).

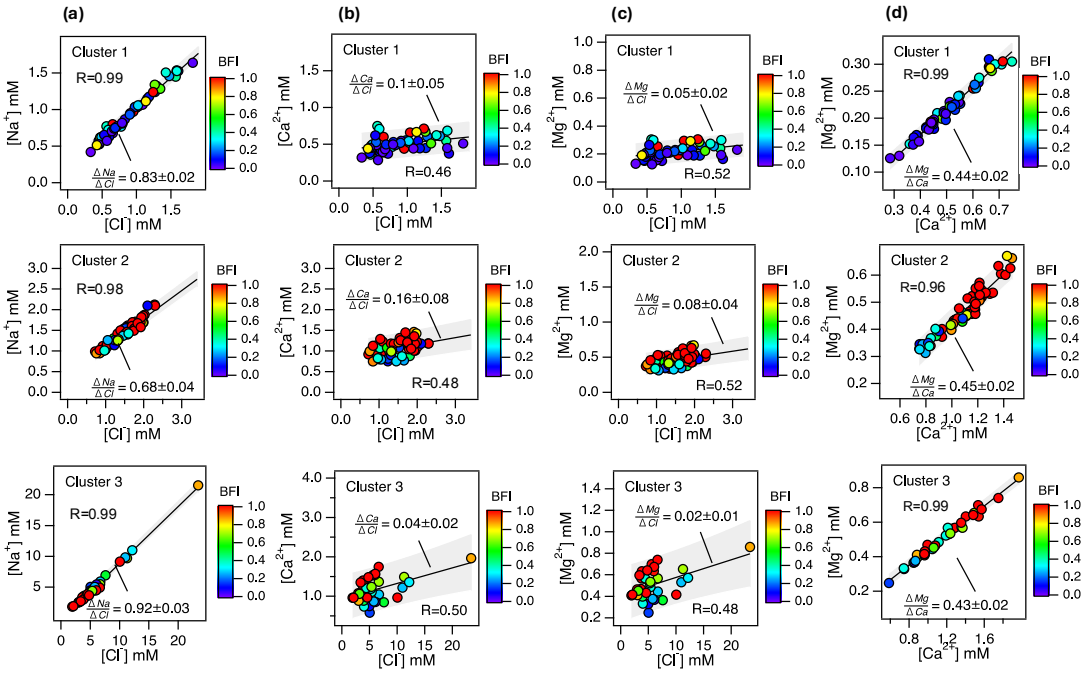

Figure S9: Cross-plots of the molar concentrations of ion pairs associate with specific deicers and anti-icers, including: (a) NaCl, (b) $CaCl_2$, (c) $MgCl_2$ and (d) ($Mg_2Ca(OAc)_6$).

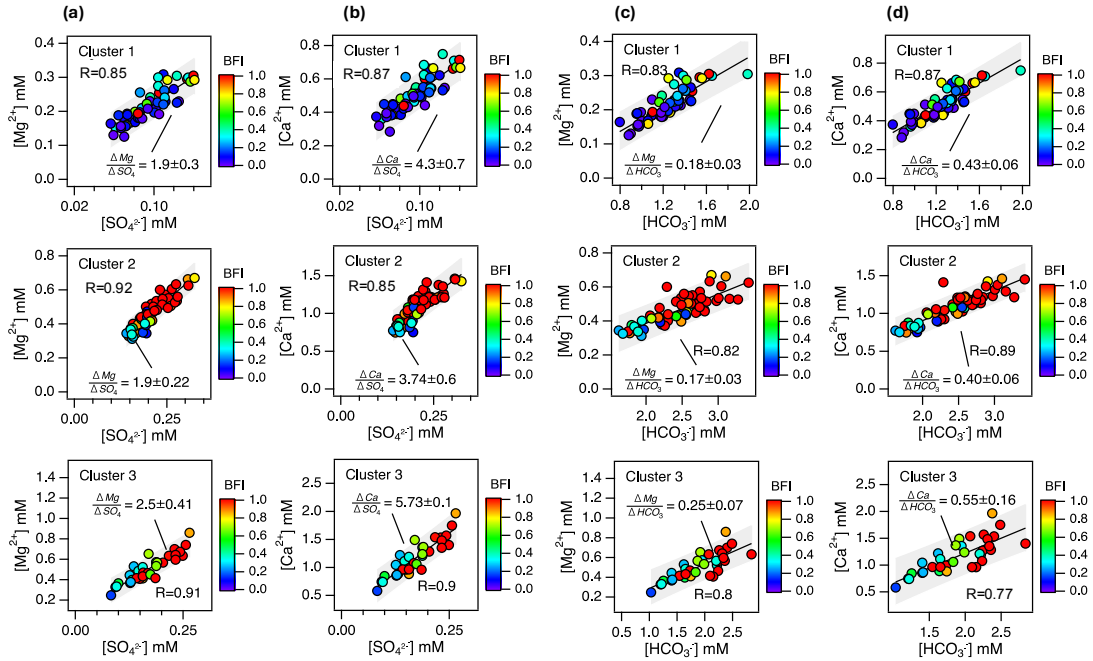

Figure S10: Cross-plots of the molar concentrations of ion pairs associate with geologic sources, including: (a) magnesium and sulfate, (b) calcium and sulfate, (c) magnesium and bicarbonate, and (d) calcium and bicarbonate.

Note S12. Nutrient Concentrations within Clusters

The concentrations, forms, and stoichiometry of N and P measured at BL30 also vary across the three clusters. The median concentration of TP—which includes dissolved inorganic PO_4^{3-} along with particulate and organic forms of P ("other-P")—is highest during summer storms (Cluster 1, Figure S11a). Cluster 1 also has elevated concentrations of PO_4^{3-} (Figure 2b in the main text) and TSS (Figure S11a) consistent with the idea that summer storms mobilize particle-associated P (e.g., from fertilized residential and urban soils, pet waste, and yard waste such as leaves and grass clippings) thereby increasing the concentrations of both dissolved PO_4^{3-} and other-P.[16–20] Yang et al.[16] noted that PO_4^{3-} was the dominant form of P in $> 90\%$ of stormwater runoff from the residential community in Florida, while in Broad Run we find that other-P, not PO_4^{3-}, is the dominant form in most baseflow and stormwater samples (i.e., median PO_4^{3-}/TP ratios are all less than 0.5 across the three clusters, Figure

S11a).

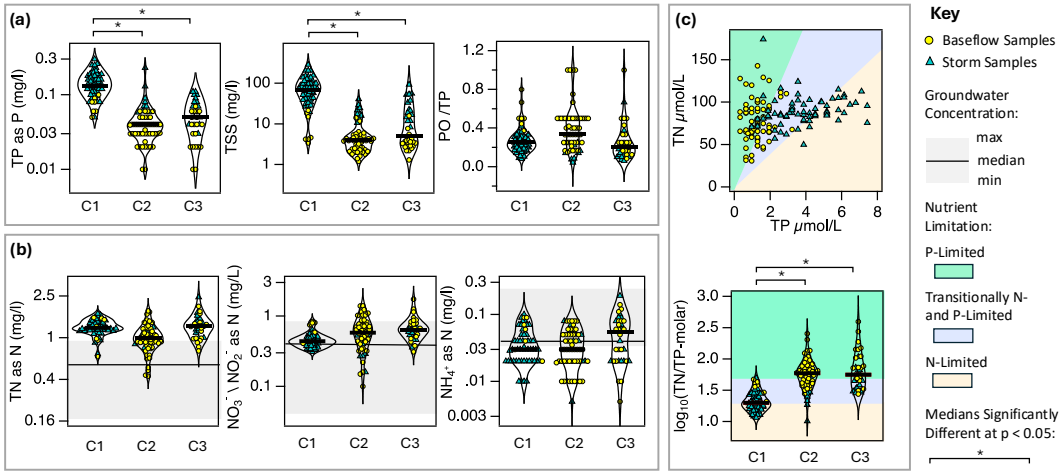

Figure S11: Breakdown by cluster of: (a) total phosphorus (TP), total suspended solids (TSS), and the fraction of TP that is dissolved orthophosphate (PO_4^{3-}); and (b) total nitrogen (TN), NO_3^-/NO_2^- (nitrate plus nitrite), and ammonium. The black horizontal lines and gray regions for TN, NO_3^-/NO_2^-, and ammonium indicate the median and range of concentrations measured in the local groundwater. Groundwater concentrations of TP and TSS were not reported. (c) The stoichiometry of TN and TP in storm and baseflow samples and by cluster. The green, purple, and orange regions in (c) represent conditions under which algal growth is likely to be P-limited (TN /TP $>$ 50), N-limited (TN/TP $<$ 20), and transitional between P- and N-limited (20 $<$ TN/TP $<$ 50), where TN and TP are expressed as molar concentrations of N and P, respectively.

Most of the TN measured at BL30 is in the form of NO_3^-/NO_2^-, and to a much lesser extent NH_4^+ (compare three graphs in Figure S11b). The median concentrations of all three forms of N evaluated here (TN, NO_3^-/NO_2^-, NH_4^+) are not significantly different across the three clusters but are similar to local groundwater concentrations (Figure S11b).

Based on a global assessment of algal growth in freshwater lakes and oceans, Guildford and Hecky[21] proposed a set of stoichiometric relationships for TN and TP when algal growth is P-limited (TN/TP $>$ 50), N-limited (TN/TP $<$ 20), or transitional between N and P limited (20 $<$ TN/TP $<$ 50), where TN and TP are expressed as molar concentrations

of N and P, respectively. Similar stoichiometric N and P thresholds have been applied to stormwater runoff.[20]

Applied to our Broad Run dataset, we find that a subset of baseflow samples fall in the P-limited range, a subset of the storm samples fall in the N-limited region, and a subset of both storm and baseflow samples are transitionally P- and N-limited (top graph, Figure S11c). Roughly half of the stream samples collected during summer storms (Cluster 1) are N-limited while the other half are transitionally N- and P-limited (bottom graph, Figure S11c). On the other hand, about half of samples collected during baseflow (Cluster 2) and during winter snow-melt or rain-on-snow events (Cluster 3) are P-limited, while the other half are transitionally N- and P-limited.

Note S13. Ion and Nutrient Concentrations vs Flow

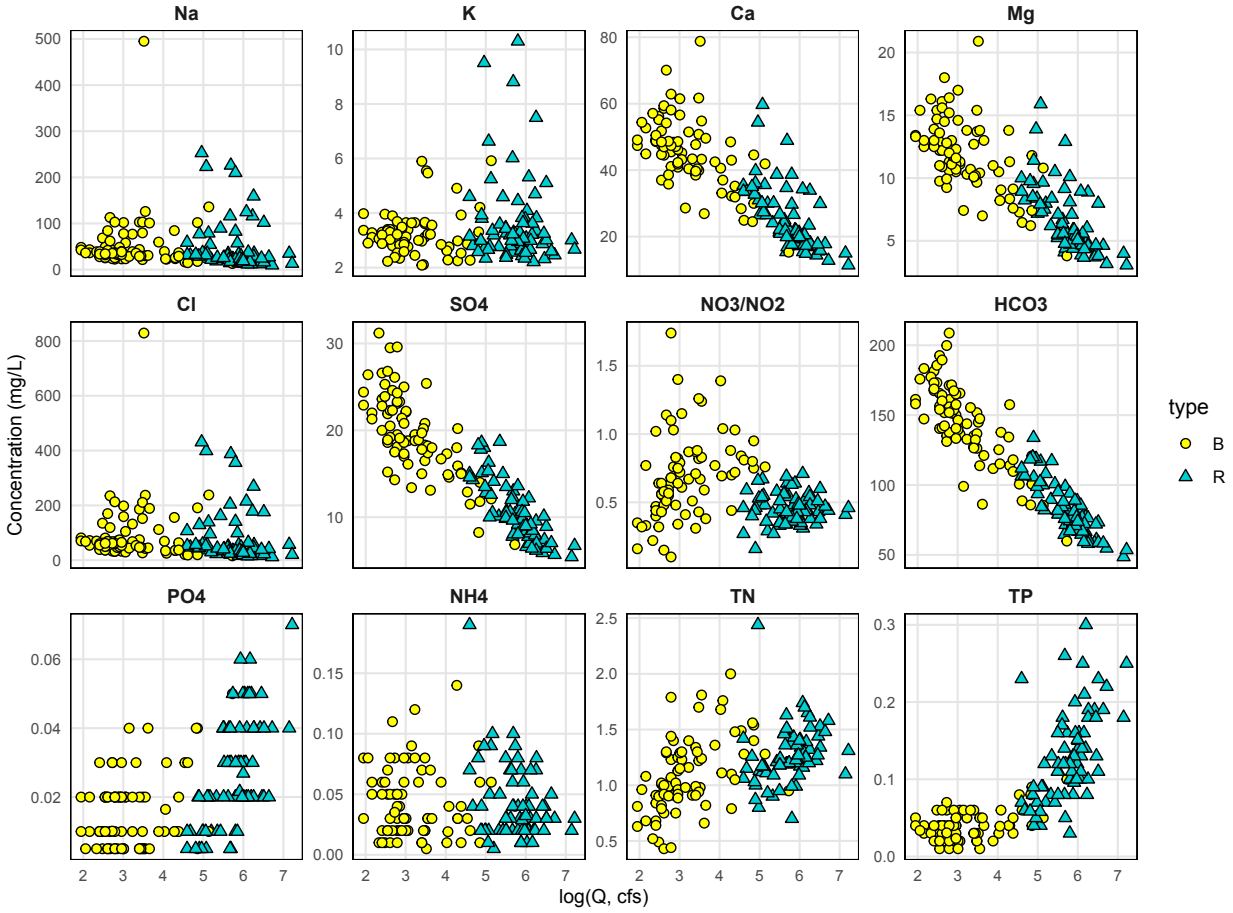

Figure S12: Concentrations of major ions and nutrients plotted against log-transformed discharge for baseflow (yellow circles) and storm flow (teal triangles) samples.

References

(1) Dewitz;Jon, U. G. S. National Land Cover Database (NLCD) 2019 Products (ver. 2.0 June 2021). 2021.

(2) Horton, J. D. Geologic Map of Virginia. 2017; https://mrdata.usgs.gov/geology/state/.

(3) Butler, J. N. *Solubility and pH calculations: the mathematics of the simplest ionic equilibria*; Addison-Wesley Reading, MA, 1964.

(4) Katz, B. G.; Collins, J. J. *Evaluation of chemical data from selected sites in the Surface-Water Ambient Monitoring Program (SWAMP) in Florida*; US Geological Survey, 1998; Vol. 98.

(5) Zeileis, A.; Grothendieck, G. **zoo** : *S3* Infrastructure for Regular and Irregular Time Series. *Journal of Statistical Software* **2005**, *14*.

(6) Eike, L. ChillR: Statistical methods for Phenology Analysis in Temperate Fruit trees. 2020; https://CRAN.R-project.org/package=chillR.

(7) Li, L.; Maier, H. R.; Partington, D.; Lambert, M. F.; Simmons, C. T. Performance assessment and improvement of recursive digital baseflow filters for catchments with different physical characteristics and hydrological inputs. *Environmental Modelling & Software* **2014**, *54*, 39–52.

(8) Zhang, J.; Zhang, Y.; Song, J.; Cheng, L. Evaluating relative merits of four baseflow separation methods in Eastern Australia. *Journal of Hydrology* **2017**, *549*, 252–263.

(9) Merz, R.; Parajka, J.; Blöschl, G. Time stability of catchment model parameters: Implications for climate impact analyses. *Water Resources Research* **2011**, *47*, 2010WR009505.

(10) Girons Lopez, M.; Vis, M. J. P.; Jenicek, M.; Griessinger, N.; Seibert, J. Assessing the degree of detail of temperature-based snow routines for runoff modelling in mountainous areas in central Europe. *Hydrology and Earth System Sciences* **2020**, *24*, 4441–4461.

(11) Shrestha, M.; Wang, L.; Koike, T.; Tsutsui, H.; Xue, Y.; Hirabayashi, Y. Correcting basin-scale snowfall in a mountainous basin using a distributed snowmelt model and remote-sensing data. *Hydrology and Earth System Sciences* **2014**, *18*, 747–761.

(12) Peres-Neto, P. R.; Jackson, D. A.; Somers, K. M. How many principal components?

stopping rules for determining the number of non-trivial axes revisited. *Computational Statistics & Data Analysis* **2005**, *49*, 974–997.

(13) Virginia Department of Environmental Quality *Stressor Analysis in Virginia: Data Collection and Stressor Thresholds*; 2017.

(14) Shelton, S. A.; Kaushal, S. S.; Mayer, P. M.; Shatkay, R. R.; Rippy, M. A.; Grant, S. B.; Newcomer-Johnson, T. A. Salty chemical cocktails as water quality signatures: Longitudinal trends and breakpoints along different U.S. streams. *Science of The Total Environment* **2024**, *930*, 172777.

(15) Sivers, S.; Isenberg, W.; Evans, D. *Salt Management Strategy: A Toolkit to Reduce the Environmental Impacts of Winter Maintenance Practices*; 2020.

(16) Yang, Y.-Y.; Toor, G. S. Stormwater runoff driven phosphorus transport in an urban residential catchment: Implications for protecting water quality in urban watersheds. *Scientific Reports* **2018**, *8*, 11681.

(17) Hobbie, S. E.; Finlay, J. C.; Janke, B. D.; Nidzgorski, D. A.; Millet, D. B.; Baker, L. A. Contrasting nitrogen and phosphorus budgets in urban watersheds and implications for managing urban water pollution. *Proceedings of the National Academy of Sciences* **2017**, *114*, 4177–4182.

(18) Selbig, W. R. Evaluation of leaf removal as a means to reduce nutrient concentrations and loads in urban stormwater. *Science of The Total Environment* **2016**, *571*, 124–133.

(19) Bratt, A. R.; Finlay, J. C.; Hobbie, S. E.; Janke, B. D.; Worm, A. C.; Kemmitt, K. L. Contribution of Leaf Litter to Nutrient Export during Winter Months in an Urban Residential Watershed. *Environmental Science & Technology* **2017**, *51*, 3138–3147.

(20) Yang, Y.-Y.; Toor, G. S. Sources and mechanisms of nitrate and orthophosphate trans-

port in urban stormwater runoff from residential catchments. *Water Research* **2017**, *112*, 176–184.

(21) Guildford, S. J.; Hecky, R. E. Total Nitrogen, Total Phosphorus, and Nutrient Limitation in Lakes and Oceans: Is There a Common Relationship? *Limnology and Oceanography* **2000**, *45*, 1213–1223.